Rare *b* Hadron Decays at the LHC

T. Blake,[1] T. Gershon,[1] and G. Hiller[2]

[1]Department of Physics, University of Warwick, Coventry CV4 7AL, United Kingdom

[2]Institut für Physik, Technische Universität Dortmund, D-44221 Dortmund, Germany

Annu. Rev. Nucl. Part. Sci. 2015. 65:113–43

First published online as a Review in Advance on May 13, 2015

The *Annual Review of Nuclear and Particle Science* is online at nucl.annualreviews.org

This article's doi: 10.1146/annurev-nucl-102014-022231

Keywords

quark flavor physics, CKM matrix, rare decays, Large Hadron Collider, Wilson coefficients

Abstract

With the completion of Run I of the CERN Large Hadron Collider, particle physics has entered a new era. The production of unprecedented numbers of heavy-flavored hadrons in high-energy proton–proton collisions allows detailed studies of flavor-changing processes. The increasingly precise measurements allow the Standard Model to be tested with a new level of accuracy. Rare *b* hadron decays provide some of the most promising approaches for such tests because there are several observables that can be cleanly interpreted from a theoretical viewpoint. In this article, we review the status and prospects in this field, with a focus on precision measurements and null tests.

Contents

1. INTRODUCTION

Among the most distinctive features of the Standard Model (SM) of particle physics is the organization of "flavors" of quarks and leptons. Flavor changes can occur only through the charged-current weak interaction, so transitions between fermions of the same charge can occur only through loop processes (1). The probabilities of different transitions are governed by the elements of the appropriate fermion mixing matrices. In particular, the fact that the Cabibbo–Kobayashi–Maskawa (CKM) quark-mixing matrix (2, 3) is approximately diagonal suppresses generation-changing transitions.

Consequently, processes involving flavor changes between two up-type (u, c, t) or between two down-type (d, s, b) quarks—that is, processes involving a generation-changing neutral current (FCNC)—occur only at loop level and are predicted to be rare within the SM. Decays of b hadrons into final states containing a photon or a dilepton pair (e^+e^-, $\mu^+\mu^-$) are of particular interest and are the main topic of this review. The rates and various kinematic distributions as well as CP asymmetries, and other properties, of such rare decays can be predicted in the SM with low theoretical uncertainty, while the measured quantities may be affected by physics beyond the Standard Model (BSM), also referred to as New Physics (NP). Comparisons between the predictions and the measurements therefore provide sensitive tests for BSM contributions.

This reason for interest in b hadron decays has been known since before the discovery of the b quark itself, and rare decays have been investigated by a number of experiments. The discovery of the $b \to s\gamma$ process by the CLEO experiment (4) has been followed by increasingly precise determinations culminating in results from the BaBar (5, 6) and Belle (7) experiments. The consistency of these measurements with the latest theoretical prediction (8) provides strong constraints on BSM models. Among the many other important results from the B factory experiments, the first evidence for the $B^+ \to \tau^+\nu_\tau$ decay (9–13) is particularly germane to this discussion. The

overall picture is one of consistency with the SM, but at a level of precision that mandates further experimental investigation.

The Large Hadron Collider (LHC) at CERN (14) provides the opportunity to make the next leap in precision. Its high-energy proton–proton collisions provide a large cross section of $\mathcal{O}(100\,\mu b)$ (15) for production of b quarks. The high luminosity delivered by the LHC enables the decay products of the b hadrons that emerge from fragmentation to be recorded in sufficient quantities to allow studies of rare decays by the ATLAS (16), CMS (17), and LHCb (18) experiments. For ATLAS and CMS, which instrument the central region of pseudorapidity, the online selection (trigger) requirements select only b hadron decays that contain a dimuon pair. The LHCb detector, however, covers the forward region, where b production peaks, and is designed to enable triggering on a broader range of b hadron decays, including those containing a photon or a dielectron pair. To achieve this goal, however, LHCb must operate at a lower instantaneous luminosity than the other experiments. In the LHC Run I data-taking period, corresponding to the calendar year (2011) 2012, when collisions were at center-of-mass energies of (7 TeV) 8 TeV, ATLAS and CMS each recorded approximately (5 fb^{-1}) 20 fb^{-1}, whereas LHCb collected around (1 fb^{-1}) 2 fb^{-1}. These data samples contain unprecedented yields of numerous interesting rare decays of b hadrons, as discussed below.

The focus of this review is the impact of the results, in the field of rare decays of b hadrons, from Run I of the LHC. We also discuss relevant results from other experiments and include a forward look to Run II and beyond. In order to find small deviations from the SM predictions, it is essential to aim for high precision; therefore, observables that can be both cleanly predicted and well measured are of the greatest interest. Such observables include relative and absolute rates, properties of kinematic distributions, and *CP* asymmetries of decays involving a dilepton pair or a photon in the final state. Certain processes that provide null tests of the SM, for example, lepton flavor– or lepton number–violating decays, are also relevant in this context. This selection of observables does not include all interesting measurements in quark flavor physics, or even in B physics. The interested reader is referred to reviews covering *CP* violation in hadronic b hadron decays (19–21), the B_s^0 system (22), D physics (23), rare kaon decays (24, 25), and t quark properties (26, 27). An earlier review on rare b hadron decays can be found in Reference 28.

The remainder of the review is organized as follows. In Section 2, we set out the theoretical framework, and in Section 3 we summarize the experimental results. We bring these two aspects together in Section 4 to enable interpretation of the results in the context of the SM and BSM theories. We conclude the review in Section 5 with a brief summary.

2. THEORETICAL FRAMEWORK

The main challenges in developing the theory of rare b decays in the LHC era are to improve precision of the predictions and to perform and refine interpretations of the data in order to map the borders of the SM and possibly detail BSM features. The focus is on exclusive decays of b hadrons, including B_s^0 mesons and b baryons. With regard to the predictions, theory greatly benefits from the determination of crucial input such as quark mixing and masses from earlier experiments, as well as from maturing heavy-quark methods applied to precision calculations of decay amplitudes. These methods are based on the separation in energy scale between the mass of the b quark and the energy scale of QCD ($m_b \gg \Lambda_{\rm QCD}$). It is also possible to construct observables that are intrinsically robust against theoretical uncertainties and, hence, provide precise tests of the SM with clean interpretation. This section outlines the framework for these tests. In Section 2.1, we introduce the effective low-energy Hamiltonian, whose induced couplings (the so-called Wilson coefficients) can be used to describe the phenomenology of a wide range of decay modes. The status

and recent advances of methods to determine QCD effects, in particular in exclusive $b \to s\ell^+\ell^-$ decays, are briefly reviewed in Section 2.2. In Section 2.3, we describe the optimized observables that are investigated experimentally, and discuss consistency checks based on symmetry relations. Finally, in Section 2.4 we describe several explicit BSM theories as examples of how deviations from the SM may appear in experiments.

2.1. Model-Independent Analysis of $b \to s$ Transitions

The large masses of the $W^\pm$ bosons, Z boson, and t quark compared with that of the b quark allow the construction of a low-energy effective field theory for $|\Delta B| = |\Delta S| = 1$ transitions, with the Hamiltonian

$$\mathcal{H}_{\text{eff}} = -\frac{4\,G_{\text{F}}}{\sqrt{2}} V_{tb} V_{ts}^* \frac{\alpha_e}{4\pi} \sum_i C_i(\mu_s)\mathcal{O}_i(\mu_s). \qquad 1.$$

Here, G_{F} is the Fermi constant, V_{ij} are CKM matrix elements, and α_e is the fine-structure constant. The $C_i(\mu_s)$ are Wilson coefficients corresponding to local operators with different Lorentz structure $\mathcal{O}_i(\mu_s)$. The operators and their Wilson coefficients are evaluated at the renormalization scale μ_s. Doubly Cabibbo-suppressed contributions to the Hamiltonian $\propto V_{ub}V_{us}^*$ have been neglected. Details of the effective Hamiltonian of Equation 1 can be found in, for example, References 29 and 30.

The following local operators are important for rare radiative, leptonic, and semileptonic b hadron decays:

$$\begin{aligned}
\mathcal{O}_7 &= \frac{m_b}{e}\bar{s}\sigma^{\mu\nu}P_{\text{R}}b\,F_{\mu\nu}, & \mathcal{O}'_7 &= \frac{m_b}{e}\bar{s}\sigma^{\mu\nu}P_{\text{L}}b\,F_{\mu\nu},\\
\mathcal{O}_8 &= g_s\frac{m_b}{e^2}\bar{s}\sigma^{\mu\nu}P_{\text{R}}T^a b\,G^a_{\mu\nu}, & \mathcal{O}'_8 &= g_s\frac{m_b}{e^2}\bar{s}\sigma^{\mu\nu}P_{\text{L}}T^a b\,G^a_{\mu\nu},\\
\mathcal{O}_9 &= \bar{s}\gamma_\mu P_{\text{L}}b\,\bar{\ell}\gamma^\mu\ell, & \mathcal{O}'_9 &= \bar{s}\gamma_\mu P_{\text{R}}b\,\bar{\ell}\gamma^\mu\ell,\\
\mathcal{O}_{10} &= \bar{s}\gamma_\mu P_{\text{L}}b\,\bar{\ell}\gamma^\mu\gamma_5\ell, & \mathcal{O}'_{10} &= \bar{s}\gamma_\mu P_{\text{R}}b\,\bar{\ell}\gamma^\mu\gamma_5\ell.
\end{aligned} \qquad 2.$$

Here, $P_{\text{L/R}} = (1 \mp \gamma_5)/2$ denotes a left/right-handed chiral projection, T^a represents the generators of QCD, and $F_{\mu\nu}$ ($G^a_{\mu\nu}$) is the electromagnetic (chromomagnetic) field-strength tensor. The chirality-flipped operators $\mathcal{O}'_i$ correspond to right-handed couplings and are obtained from $\mathcal{O}_i$ with the replacement $P_{\text{L}} \leftrightarrow P_{\text{R}}$. The left-handedness of the charged-current interaction means that the Wilson coefficients C'_i corresponding to these primed operators are suppressed by $\mathcal{O}(m_s/m_b)$ in the SM.

The Wilson coefficients $C_i^{(\prime)}$ can be determined from measurements of observables in various different b hadron decay channels. Among the operators of Equation 2, radiative b hadron decays receive contributions from $\mathcal{O}_7^{(\prime)}$ and purely leptonic decays from $\mathcal{O}_{10}^{(\prime)}$. Semileptonic $b \to s\ell^+\ell^-$ decays receive contributions from all $\mathcal{O}_7^{(\prime)}$, $\mathcal{O}_9^{(\prime)}$, and $\mathcal{O}_{10}^{(\prime)}$. The $b \to d\gamma$ and $b \to d\ell^+\ell^-$ transitions are treated analogously but are further suppressed by $V_{tb}V_{td}^*$, as opposed to $V_{tb}V_{ts}^*$ in Equation 1. Consequently, in $b \to d$ transitions, *CP*-violating effects are generically larger because $V_{ub}V_{ud}^*$ is of comparable magnitude to $V_{tb}V_{td}^*$, though the stronger GIM (Glashow–Iliopoulos–Maiani) suppression (1) of the $V_{ub}V_{ud}^*$ term limits the size of any *CP* asymmetry. In the SM, the scalar (S) and pseudoscalar (P) operators

$$\begin{aligned}
\mathcal{O}_{\text{S}} &= \bar{s}\,P_{\text{R}}b\,\bar{\ell}\ell, & \mathcal{O}'_{\text{S}} &= \bar{s}\,P_{\text{L}}b\,\bar{\ell}\ell,\\
\mathcal{O}_{\text{P}} &= \bar{s}\,P_{\text{R}}b\,\bar{\ell}\gamma_5\ell, & \mathcal{O}'_{\text{P}} &= \bar{s}\,P_{\text{L}}b\,\bar{\ell}\gamma_5\ell
\end{aligned} \qquad 3.$$

are highly suppressed due to the small masses of the leptons and can be safely neglected even for decays involving τ leptons. Contributions from the tensor (T) operators

$$\mathcal{O}_{\rm T} = \bar{s}\sigma_{\mu\nu} b\, \bar{\ell}\sigma^{\mu\nu}\ell, \quad \mathcal{O}_{\rm T5} = \bar{s}\sigma_{\mu\nu} b\, \bar{\ell}\sigma^{\mu\nu}\gamma_5\ell \qquad 4.$$

are also negligibly small in the SM.

The Wilson coefficients at the weak scale are obtained from matching amplitudes of the full electroweak theory onto $\mathcal{H}_{\rm eff}$. Below the W boson mass, the Wilson coefficients follow renormalization group evolution assuming SM dynamics (29). The values at $\mu_s = m_b$ are (31)

$$C_7^{\rm SM} = -0.3, \quad C_9^{\rm SM} = +4.2, \quad C_{10}^{\rm SM} = -4.2. \qquad 5.$$

Comparisons between the measured values and the predictions provide sensitive tests of the SM. BSM theories can modify the Wilson coefficients of $\mathcal{H}_{\rm eff}$ (Equation 1), including those of operators not present or suppressed in the SM: $C_i^{(\prime)} = C_i^{(\prime){\rm SM}} + C_i^{(\prime){\rm NP}}$. The number of possible new operators, at dimension six, is large and includes scalar, pseudoscalar, and tensor operators. If the BSM physics does not couple universally to leptons, then sets of operators need to be considered separately for the different lepton flavors. New operators can also, in principle, induce lepton flavor–violating processes that are forbidden by accidental symmetries of the SM. Operators can also be associated with new sources of *CP* violation, making their Wilson coefficients complex-valued. The large number of possible operators is intractable for a fully model-independent analysis. However, certain experimental signatures that can be explained only by particular extensions to the SM operator basis allow for a simplified analysis.

Recently, it has become customary to rewrite the semileptonic operators of Equation 1 in a basis with left- and right-projected leptons (32, 33):

$$\begin{aligned} \mathcal{O}_{\rm LL} &\equiv (\mathcal{O}_9 - \mathcal{O}_{10})/2, \quad \mathcal{O}_{\rm LR} \equiv (\mathcal{O}_9 + \mathcal{O}_{10})/2, \\ \mathcal{O}_{\rm RL} &\equiv (\mathcal{O}'_9 - \mathcal{O}'_{10})/2, \quad \mathcal{O}_{\rm RR} \equiv (\mathcal{O}'_9 + \mathcal{O}'_{10})/2, \end{aligned} \qquad 6.$$

where

$$\begin{aligned} C_{\rm LL} &= C_9 - C_{10}, \quad C_{\rm LR} = C_9 + C_{10}, \\ C_{\rm RL} &= C'_9 - C'_{10}, \quad C_{\rm RR} = C'_9 + C'_{10}. \end{aligned} \qquad 7.$$

This basis change is useful in frameworks wherein BSM physics at a high mass scale respects the $SU(2)_{\rm L}$ part of the SM gauge symmetry group, resulting in a simpler structure. For instance, fitting the two parameters C_9 and C_{10}, if it is assumed that BSM physics contributes to LL only, the constraint $C_9 + C_{10} = 0$ can be used. In addition, $SU(2)_{\rm L}$ relations between b decay observables and t quark physics can be obtained (34).

2.2. Nonhadronic *b* Hadron Decays in QCD

Semileptonic heavy-to-light b hadron decays such as $B^0 \to K^{*0}\mu^+\mu^-$ have particularly interesting phenomenology. These decays have sensitivity to electroweak physics in two kinematic regimes: (*a*) At low invariant dilepton mass squared (q^2), where the emitted hadron is energetic ($E \gg \Lambda_{\rm QCD}$ in the b hadron rest frame), QCD factorization (QCDF) applies (35), and (*b*) at high invariant dilepton mass, the region of low hadronic recoil, where $q^2 = \mathcal{O}(m_b^2)$, an operator product expansion (OPE) in $1/m_b$ applies (36). **Figure 1** depicts these different kinematic regimes. In both cases, the heavy-to-light decays can be predicted systematically from QCD. The methods used for such predictions are now commonly employed in the field, and in view of the experimental situation, control of uncertainties becomes central. The dominant systematic uncertainties are

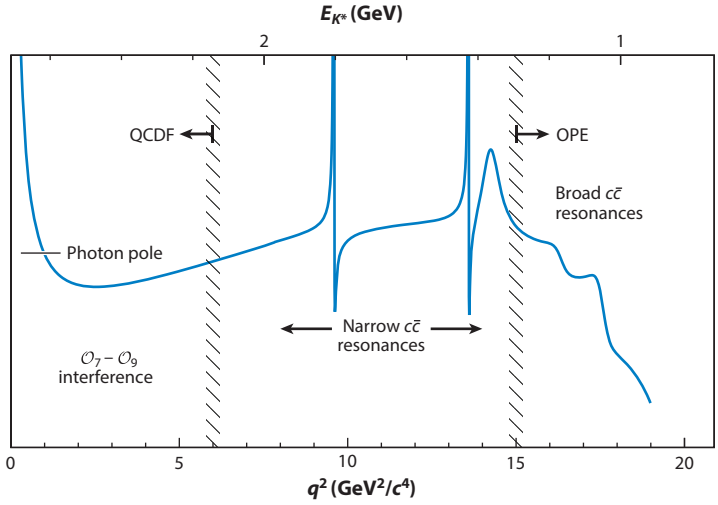

Figure 1

Sketch of the differential decay rate of $B^0 \to K^{*0}\mu^+\mu^-$ as a function of q^2. At very low q^2 (near maximal E_{K^*}), the virtual photon contribution associated with $C_7^{(\prime)}$ dominates. As q^2 increases, in the region $1 < q^2 < 6\,\mathrm{GeV}^2/c^4$ interference between $\mathcal{O}_7$ and $\mathcal{O}_9$ increases, providing excellent sensitivity to New Physics in C_9. At intermediate q^2, the spectrum is dominated by the narrow J/ψ and $\psi(2S)$ resonances. At large q^2 (small E_{K^*}), contributions from broad charmonium resonances, above the open charm threshold, can be treated with a local operator product expansion (OPE).

parametric uncertainties from the hadronic transition form factors, $1/m_b$ power corrections (at low q^2), and backgrounds from $c\bar{c}$ resonances above the open charm threshold (at high q^2). In light of these issues, it is mandatory to study the low- and high-q^2 regions separately, and it has become conventional to perform analyses in finer bins of q^2.

The transition form factors for heavy-to-light decays can be computed using the method of light-cone sum rules (LCSR) if the final-state hadronic system is energetic. Determinations for $B \to K$ and $B \to K^*$ form factors can be found in Reference 37 and References 38 and 39, respectively. Recently, it has also become possible to determine the same form factors from lattice gauge theory. Lattice calculations are applicable only when the hadron is almost at rest in the b hadron decay frame—that is, at low recoil. The LCSR and lattice results therefore complement one another, covering different kinematic regimes. Unquenched lattice determinations can be found for $B \to K$ (40), $B \to K^*$ and $B_s^0 \to \phi$ (41), and $\Lambda_b^0 \to \Lambda$ (42) form factors. All lattice and most LCSR determinations assume that the light particle being produced is both narrow and stable. This may not be a good approximation in some cases, in particular for the $B \to K^*$ transition due to the large width of the K^* resonance. There are prospects for an improved treatment in future lattice calculations (43).

Issues of $1/m_b$ corrections exist for low q^2 only because the power corrections at high q^2 are parametrically suppressed, bringing them to the few-percent level. The topic of power corrections has received a great deal of recent attention (44–46). Eventually, it will be possible to determine the corrections from data (47) or to subject them to consistency checks, as discussed in Section 2.3, below.

Amplitudes for rare semileptonic decays also receive contributions from the more prevalent b hadron decays to final states containing charmonia, through the quark-level transition $b \to c\bar{c}s$,

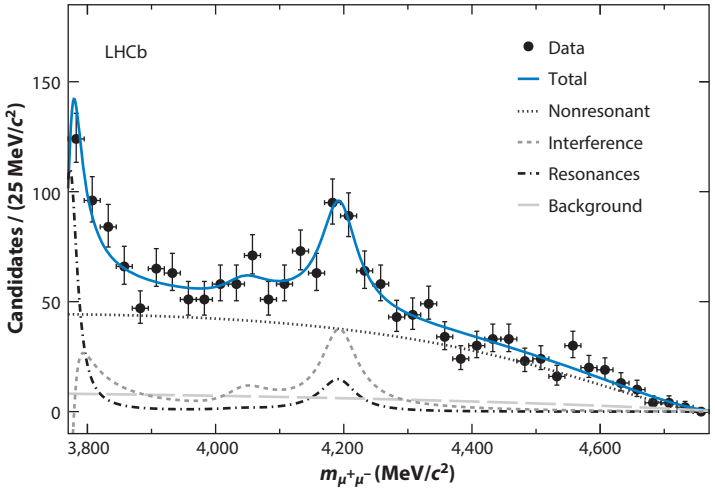

Figure 2

Background-subtracted dimuon mass distribution of $B^+ \to K^+\mu^+\mu^-$ candidates (51). Broad resonant contributions from the decays $B^+ \to \psi(3770)K^+$ and $B^+ \to \psi(4160)K^+$ are clearly visible.

where the $c\bar{c}$ resonance subsequently decays into dileptons. In the effective theory, such contributions are induced by four-quark operators:

$$\mathcal{O}_1 = \frac{4\pi}{\alpha_e}\bar{s}\gamma_\mu P_L b\, \bar{c}\gamma^\mu P_L c, \quad \mathcal{O}_2 = \frac{4\pi}{\alpha_e}\bar{s}\gamma_\mu P_L c\, \bar{c}\gamma^\mu P_L b. \qquad 8.$$

These operators arise predominantly from tree-level W boson exchange and have large, order-one Wilson coefficients at the b quark scale: $C_1 \sim -0.2$, $C_2 \sim 1.1$. The most prominent effect of charmonia in semileptonic decays is the narrow resonance peaks at $q^2 = m^2_{J/\psi}, m^2_{\psi(2S)}$ (**Figure 1**); in experimental analyses these q^2 regions have to be removed. In principle, however, the presence of charmonia affects the entire q^2 region. In radiative decays and at large recoil, all charmonia are off-shell and are suppressed (37, 48). At high q^2 values, a number of broad $c\bar{c}$ resonances can contribute (49, 50). Such structure has been measured quite precisely in the $B^+ \to K^+\mu^+\mu^-$ decay (**Figure 2**) (51). Under a naïve factorization assumption, this structure can be compared with that from $e^+e^- \to$ hadrons (52, 53) by use of dispersion relations (49). Such a comparison (54) revealed a dramatic deviation from expectation. Although naïve factorization is not expected to be valid at high precision, this surprising difference needs to be understood in order to maximize the sensitivity to NP.

For completeness, we note that there are also contributions from four-quark operators, referred to as QCD penguins, with flavor structure $\mathcal{O}_{3..6} \sim \bar{s}\gamma_\mu P_L b \sum_{u,d,s,c,b} \bar{q}\gamma^\mu P_{L,R} q$. Their SM Wilson coefficients at the m_b scale are small, $\mathcal{O}(10^{-2})$; therefore, their effects in radiative and semileptonic b hadron decays are generally small. However, contributions from light resonances such as the ϕ meson, mediated by these operators, will become important as the precision improves.

The OPE does not describe the resonance contributions locally in the amplitudes (55). It is, however, expected to capture their effect after integrating over a sufficient range of q^2. Thus, it is important to investigate the optimal binning for precision BSM searches. As the OPE does predict universality between certain transversity amplitudes, cancellation of the effects of resonances is expected in particular ratios (56).

2.3. Optimized Observables and Symmetry Relations

Semileptonic $b \to s\ell^+\ell^-$ decays with a vector meson in the final state provide a particularly rich set of observables that can be accessed through the angular distribution of the particles in the decay. The decay rate for these semileptonic processes can be expressed in terms of decay amplitudes for the vector mesons corresponding to different transversity states: $A_\parallel^{\mathrm{L,R}}$, $A_\perp^{\mathrm{L,R}}$, and $A_0^{\mathrm{L,R}}$. The axial–vector coupling through C_{10} allows one to distinguish between amplitudes with left- and right-handed chirality of the dilepton system. For completeness, we note that a fourth amplitude (A_t) exists that corresponds to the spin-zero $\ell^+\ell^-$ configuration. The effect of this amplitude, however, is suppressed by the small lepton mass. In BSM models with (pseudo)scalar operators, the effect of A_t can be enhanced, and a further amplitude, A_{S}, appears. In the presence of tensor operators, six additional transversity amplitudes can enter (57).

It is then possible to construct angular observables that are related to these decay amplitudes, for example, the fraction of the longitudinal polarization of the vector meson:

$$F_{\mathrm{L}} = \frac{|A_0^{\mathrm{L}}|^2 + |A_0^{\mathrm{R}}|^2}{|A_0^{\mathrm{L}}|^2 + |A_0^{\mathrm{R}}|^2 + |A_\parallel^{\mathrm{L}}|^2 + |A_\parallel^{\mathrm{R}}|^2 + |A_\perp^{\mathrm{L}}|^2 + |A_\perp^{\mathrm{R}}|^2}. \qquad 9.$$

One of the most widely discussed observables is the forward–backward asymmetry of the dilepton system,

$$A_{\mathrm{FB}} = \frac{4}{3}\frac{\mathrm{Re}\left(A_\parallel^{\mathrm{L}} A_\perp^{\mathrm{L}*} - A_\parallel^{\mathrm{R}} A_\perp^{\mathrm{R}*}\right)}{|A_0^{\mathrm{L}}|^2 + |A_0^{\mathrm{R}}|^2 + |A_\parallel^{\mathrm{L}}|^2 + |A_\parallel^{\mathrm{R}}|^2 + |A_\perp^{\mathrm{L}}|^2 + |A_\perp^{\mathrm{R}}|^2}, \qquad 10.$$

which arises from the chiral nature of the coupling to the leptons and flips its sign at $q^2 \approx 4\,\mathrm{GeV}^2/c^4$ (35, 58, 59) due to interference between the photon dipole ($\mathcal{O}_7^{(\prime)}$) and vector operators ($\mathcal{O}_9^{(\prime)}$).

It is also possible to build sets of "optimized" observables from the decay amplitudes in which the leading form factor uncertainties cancel. The design of such observables is based on the $1/m_b$ expansion. In both kinematic regions of interest (low q^2 and high q^2), the transversity amplitudes receive their leading contribution from a factorizable form factor term,

$$A_i^{\mathrm{L,R}} = f_i \times C_i^{\mathrm{L,R}} + \text{nonfactorizable}, \quad i = 0,\ \parallel, \text{or } \perp, \qquad 11.$$

where the f_i are corresponding transversity form factors and contain long-distance (QCD) information only. The $C_i^{\mathrm{L,R}}$ denote short-distance coefficients, which are sensitive to electroweak-scale physics. They are composed of Wilson coefficients of the semileptonic four-fermion operators as well as contributions from four-quark and dipole operators (see Section 2.1).

At low q^2, the form factor relations imply that $f_\parallel = f_\perp + \mathcal{O}(1/m_b)$, such that $A_\parallel^{\mathrm{L,R}} \approx -A_\perp^{\mathrm{L,R}}$ if $C' = 0$. This relationship allows one to construct SM null tests with sensitivity to right-handed currents, for example (60),

$$A_{\mathrm{T}}^{(2)} = \frac{|A_\perp^{\mathrm{L}}|^2 + |A_\perp^{\mathrm{R}}|^2 - |A_\parallel^{\mathrm{L}}|^2 - |A_\parallel^{\mathrm{R}}|^2}{|A_\perp^{\mathrm{L}}|^2 + |A_\perp^{\mathrm{R}}|^2 + |A_\parallel^{\mathrm{L}}|^2 + |A_\parallel^{\mathrm{R}}|^2}, \qquad 12.$$

which is expected to be very close to zero in the SM. It is also possible to build other clean observables from bilinear combinations of amplitudes such that $f_\parallel$, $f_\perp$, and f_0 cancel at leading order in $1/m_b$. The P' family (61) is a good example of a set of these clean observables, for instance,

$$\begin{aligned} P_5' &= \sqrt{2}\frac{\mathrm{Re}\left(A_0^{\mathrm{L}} A_\perp^{\mathrm{L}*} - A_0^{\mathrm{R}} A_\perp^{\mathrm{R}*}\right)}{\sqrt{\left(|A_0^{\mathrm{L}}|^2 + |A_0^{\mathrm{R}}|^2\right)\left(|A_\parallel^{\mathrm{L}}|^2 + |A_\parallel^{\mathrm{R}}|^2 + |A_\perp^{\mathrm{L}}|^2 + |A_\perp^{\mathrm{R}}|^2\right)}}, \\ &\approx \sqrt{2}\frac{\mathrm{Re}\left(C_0^{\mathrm{L}} C_\perp^{\mathrm{L}} - C_0^{\mathrm{R}} C_\perp^{\mathrm{R}}\right)}{\sqrt{\left(|C_0^{\mathrm{L}}|^2 + |C_0^{\mathrm{L}}|^2\right)\left(|C_\perp^{\mathrm{L}}|^2 + |C_\perp^{\mathrm{L}}|^2 + |C_\parallel^{\mathrm{L}}|^2 + |C_\parallel^{\mathrm{L}}|^2\right)}}. \end{aligned} \qquad 13.$$

Table 1 Data on $B \to K^* \ell^+ \ell^-$ and $B_s^0 \to \phi \ell^+ \ell^-$ in the endpoint bin $q^2 \in [16, 19]$ GeV$^2/c^4$ (LHC experiments) or otherwise $q^2 \in [16\,\text{GeV}^2/c^4, q^2_{\text{max}}]$ versus the endpoint prediction[a]

	F_L	S_3	P_4'	S_7	P_5'/A_{FB}	S_8/S_9
Endpoint	1/3	−1/3	$\sqrt{2}$	0	$\sqrt{2}$	−1/2
$B \to K^* \ell^+ \ell^-$	0.38 ± 0.04	-0.22 ± 0.09	$0.70^{+0.44}_{-0.52}$	$0.15^{+0.16}_{-0.15}$	1.63 ± 0.57	-0.5 ± 2.2
$B_s^0 \to \phi \ell^+ \ell^-$	$0.16^{+0.18}_{-0.12}$	$0.19^{+0.30}_{-0.31}$	—	—	—	—

[a]Note that $S_3 = 1/2(1 - F_L)A_T^{(2)}$. Dashes indicate that no data are presently available. Adapted from Reference 56.

At high q^2, the OPE predicts a different kind of relationship:

$$A_{\parallel,0}^{L,R} = f_{\parallel,0} \times C_-^{L,R}, \quad A_\perp^{L,R} = f_\perp C_+^{L,R}, \qquad C_-^{L,R} = C_+^{L,R} \quad \text{if and only if} \quad C' = 0. \tag{14.}$$

It follows immediately that the ratio $A_0^{L,R}/A_\parallel^{L,R}$ is free of short-distance effects—in other words, independent of C_i. This feature allows one to extract the form factor ratio $f_0/f_\parallel$ directly from the data. If there are no right-handed currents ($C' = 0$), the form factor ratio $f_\perp/f_\parallel$ can be extracted in this kinematic region from $A_T^{(2)}$. This information about the hadronic system can in turn be used to provide better control of uncertainties on other observables. One can also derive form factor–free observables at high q^2, such as the $H_T^{(i)}$ family (62).

At zero recoil, when $q^2 = (m_B - m_{K^*})^2$, there are exact relationships between the amplitudes due to ambiguity of the direction of the K^* in the B rest frame. At this kinematic endpoint, $A_\perp^{L,R} = 0$ and $A_\parallel^{L,R} = -\sqrt{2}A_0^{L,R}$ (56). The endpoint predictions can be compared with data (**Table 1**) to provide a consistency check. Parity selection allows one to extend the prediction to the vicinity of the endpoint, where observables such as A_{FB} and P_5' vary linearly with the modulus of the K^* three-momentum in the B center-of-mass frame, and the slope provides a test of the SM.

There are also more general relationships between the angular observables J of the $B \to K^* \ell^+ \ell^-$ decay (defined in Section 3.3) due to the composition of the observables in terms of pairs of transversity amplitudes. These relationships, which are valid over the whole range of q^2, serve as a further consistency check of the experimental results (63).

2.4. Benchmarking New Physics

An important motivation in the building of BSM models is the origin of electroweak symmetry breaking and the stabilization of the weak scale, namely the so-called hierarchy problem (see, e.g., Reference 64). Among the most promising approaches are models that invoke supersymmetry, extra dimensions, new strong interactions, or combinations thereof. Generically, in these models flavor violation beyond the CKM matrix is induced. Severe constraints on masses and couplings must be imposed for the NP to maintain contact with the electroweak scale: Without any suppression on flavor-changing couplings (which could be SM-like, with GIM- and CKM-like effects), NP is pushed up to scales as high as 10^5 TeV (65). In turn, the nonobservation of BSM effects in the flavor sector provides important information about NP.

2.4.1. Minimal flavor violation. SM extensions can be classified according to their degree of flavor violation. The term minimal flavor violation (MFV) is used for models in which flavor is broken in an SM-like way. Formally, within MFV the spurion fields that break the flavor symmetry that would be present in the SM in the absence of quark masses correspond to the SM Yukawa couplings (66). Thus, the flavor violation can be parameterized in terms of quark masses and CKM

elements, which are known parameters of the SM. Any deviation from MFV corresponds to NP. The MFV paradigm provides an attractive way to resolve the tension between the expectation that the NP scale should be $\mathcal{O}(1\ \text{TeV})$ due to naturalness arguments, whereas limits from FCNC processes assuming generic NP couplings point to a much higher scale. Still, viable non-MFV models exist with BSM around the TeV scale or higher.

The MFV framework can be tested through *CP*-violating observables as well as rare decays. Because the effective Hamiltonians for $b \to d$ and $b \to s$ transitions share the same structure (as discussed in Section 2.1), ratios of $b \to d$ and $b \to s$ processes provide powerful tests of MFV. Generically, one can predict that such ratios in the SM are equal to $|V_{td}/V_{ts}|^2 \approx 1/25$ modified by hadronic matrix elements and phase-space factors, whereas in non-MFV models they can take very different values. An important example is the ratio of B^0 and B_s^0 dimuon decay rates (67), but $\mathcal{B}(B^0 \to \rho\gamma)/\mathcal{B}(B^0 \to K^{*0}\gamma)$ (68, 69) and $\mathcal{B}(B^+ \to \pi^+\ell^+\ell^-)/\mathcal{B}(B^+ \to K^+\ell^+\ell^-)$ (70) exhibit similar features. To reach high precision, one needs to have good control of $SU(3)$ breaking in the hadronic matrix elements. The ratio $\mathcal{B}(B_s^0 \to \bar{K}^{*0}\ell^+\ell^-)/\mathcal{B}(B^0 \to K^{*0}\ell^+\ell^-)$ may provide a complementary approach to the control of such uncertainties.

2.4.2. Model building and simplified models. In addition to modifying FCNCs, NP models typically predict new particles that can be searched for at the LHC. Because evidence for these new particles has not been found in Run I, limits on the masses of these particles have been pushed into the TeV range (71). To keep the relation to the weak scale, without invoking any fine tuning of parameters, researchers have developed new approaches to model building (see, e.g., References 72–74).

Instead of building models that are complete up to the GUT or Planck scale, researchers commonly consider simplified models. These usually comprise the SM plus one new sector with a rather small number of new parameters, making these models predictive and easy to constrain. The choice of new sector is either made by theoretical prejudice or driven by a need to explain a deficiency of the SM or a discrepancy between SM predictions and data. Two such simplified models, motivated by current hints of discrepancies in the $B \to K^{(*)}\ell^+\ell^-$ data, are Z penguins and leptoquarks.

A Z penguin is an FCNC involving a neutral external field that originates from a $U(1)$ gauge interaction. In the case of the SM, Z penguins arise at loop level and are induced by the weak interaction. Modifications to the effective couplings arise generically in most SM extensions (75). For the $b \to s$ transition,

$$\mathcal{L}^Z = Z^\mu (g_{sb}^{\mathrm{L}} \bar{s}\gamma_\mu P_{\mathrm{L}} b + g_{sb}^{\mathrm{R}} \bar{s}\gamma_\mu P_{\mathrm{R}} b) + \text{h.c.}, \qquad 15.$$

where the couplings $g_{sb}^{\mathrm{L/R}}$, which can be related to the Wilson coefficients $C_{9,10}^{(\prime)}$, are generically complex. If the couplings to the leptons are SM-like, then the vector current coupling is suppressed relative to the axial–vector one by a factor of $|4\sin^2\theta_{\mathrm{W}} - 1|$, where θ_{W} is the weak mixing angle and the main contribution is through $C_{10}^{(\prime)}$. With $U(1)$ extensions of the SM (Z' models), however, the contribution to $C_9^{(\prime)}$ can also be sizable. An example of a Z' model is a gauge extension to $\tau-\mu$ lepton number (76, 77). A survey of the parameter space of Z' models can be found in Reference 78.

Leptoquarks are bosonic particles that carry one lepton and one quark flavor quantum number. They can have spin one but are more commonly assumed to be scalar particles (ϕ) that have Yukawa-like couplings ($\lambda_{q\ell}^{\mathrm{L}}$, $\lambda_{q\ell}^{\mathrm{R}}$) to the (left- or right-handed, respectively) SM fermions:

$$\mathcal{L}^{\mathrm{LQ}} = -\lambda_{q\ell}^{\mathrm{L}}\, \phi\, (\bar{q}\, P_{\mathrm{L}}\, \ell) - \lambda_{q\ell}^{\mathrm{R}}\, \phi\, (\bar{q}\, P_{\mathrm{R}}\, \ell) + \text{h.c.} \qquad 16.$$

Tree-level ϕ-exchange induces processes such as $b \to (s, d)\ell\ell$, which, depending on the handedness of the interaction, result in a modification of the semileptonic Wilson coefficients $C_{9,10}^{(\prime)}$

(33). Leptoquarks can also provide a natural explanation for nonuniversal couplings to leptons in $b \to s\ell^+\ell^-$ processes. Generally, leptoquarks also induce lepton flavor violation (LFV), requiring an extension to the SM operator basis. Limits on $\mathcal{B}(\mu^\pm \to e^\pm\gamma)$ and $\mathcal{B}(B^0_{(s)} \to e^\pm\mu^\mp)$ strongly constrain the couplings involving electrons and muons, but the parameter space for other couplings remains viable. With benchmark masses between 1 and 50 TeV, motivated by the hint of lepton nonuniversality discussed in Section 3.4, it would be challenging to observe directly produced leptoquarks at the LHC, but effects could be visible in rare decay processes such as $B \to K\tau^\pm\mu^\mp$ and $B^0_{(s)} \to \tau^\pm\mu^\mp$ (79–81).

3. STATUS AND PROSPECTS OF MEASUREMENTS

3.1. Dilepton Decays

In the SM, the leptonic $B^0_s \to \mu^+\mu^-$ and $B^0 \to \mu^+\mu^-$ decays are exceedingly rare. In addition to being loop and CKM suppressed, the decay of a pseudoscalar B meson into a pair of muons is significantly helicity suppressed in the SM. The SM values of the time-integrated branching fractions (82) can be expressed as (83, 84)

$$\bar{\mathcal{B}}(B^0_{(s)} \to \mu^+\mu^-) = \frac{\left|V^*_{tb}V_{tq}\right|^2 G_F^2\alpha_e^2\, M_{B^0_{(s)}} M_\mu^2 f^2_{B^0_{(s)}}}{16\pi^3\Gamma_{q\mathrm{H}}} \sqrt{1-\frac{4M_\mu^2}{M^2_{B^0_{(s)}}}}\left|C_{10}(m_b)\right|^2 + \ldots, \qquad 17.$$

where the ellipsis denotes subleading terms, M denotes the mass of the particle in subscript, and $\Gamma_{q\mathrm{H}}$ is the total width of the heavier of the two mass eigenstates in the $B^0_{(s)}$–$\bar{B}^0_{(s)}$ system. Whereas all those quantities are well known from experiments, the decay constant $f_{B^0_{(s)}}$ must be determined from lattice QCD. Using values of $f_{B^0_{(s)}}$ obtained by averaging different calculations (85–88) and including higher-order QCD and electroweak corrections (89, 90), one obtains the latest SM predictions (84):

$$\begin{aligned}\bar{\mathcal{B}}(B^0_s \to \mu^+\mu^-) &= (3.65 \pm 0.23) \times 10^{-9},\\ \bar{\mathcal{B}}(B^0 \to \mu^+\mu^-) &= (1.06 \pm 0.09) \times 10^{-10}.\end{aligned} \qquad 18.$$

The uncertainties on the SM predictions come mainly from the knowledge of the decay constants and the CKM matrix elements. In both cases, improvement can be anticipated with refined lattice QCD calculations.

The suppression of the $B^0_{(s)} \to \mu^+\mu^-$ branching fractions is characteristic of the SM. In particular, scalar contributions from SM Higgs penguin diagrams are negligible due to the small muon mass. However, many BSM models can cause the branching fractions to deviate from their SM values. Models with extended Higgs sectors, for example, can produce significant enhancements in the rates of the decays as the helicity suppression is broken (see, e.g., References 91–94). The ratio of branching fractions for B^0 and B^0_s decays to dimuons also provides a stringent test of MFV.

Prior to data-taking at the LHC, no evidence for either decay had been found, and limits on these decays' branching fractions were still an order of magnitude above the SM expectations (95, 96). A series of results from the LHC experiments (97–101) significantly restricted the available phase space for BSM theories, providing strong constraints complementary to those from searches for on-shell production of new particles. In summer 2013, both CMS (102) and LHCb (103) reported evidence of the $B^0_s \to \mu^+\mu^-$ decay at the level of four standard deviations (4σ) using their full Run I data sets. These experiments exploited multivariate event classifiers to optimize the separation of signal from backgrounds consisting of muons from different b hadron decays. Backgrounds from b hadron decays in which one or more particles were mistakenly identified as

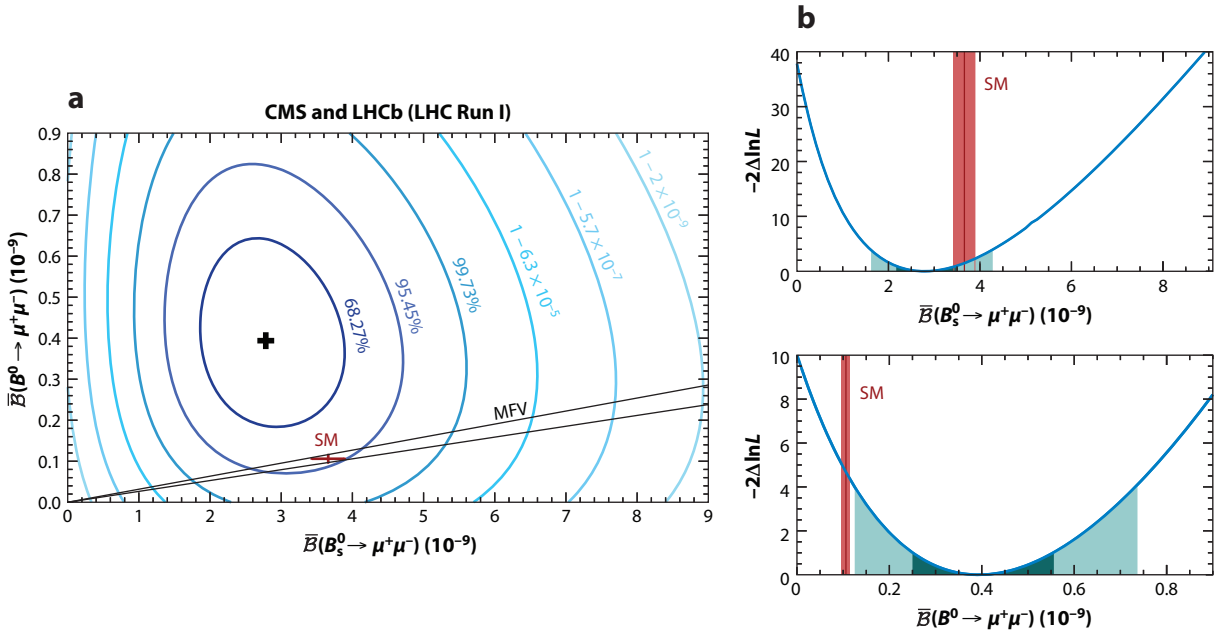

Figure 3

(*a*) Likelihood contours for the $B_s^0 \to \mu^+\mu^-$ and $B^0 \to \mu^+\mu^-$ branching fractions from a fit to the combined LHCb and CMS data sets. The cross indicates the best-fit point in the two-dimensional plane of the branching fractions, where the Standard Model (SM) and minimal flavor violation (MFV) predictions are also shown. (*b*) The one-dimensional projections of the likelihood are also shown. Modified from Reference 104.

muons or in which one or more particles from a *b* hadron decay were not reconstructed were estimated using samples of simulated events whose performance had been corrected to match that of the data.

To obtain the best information from the LHC Run I data set, CMS and LHCb (104) simultaneously analyzed both data sets, yielding

$$\begin{aligned} \bar{\mathcal{B}}(B_s^0 \to \mu^+\mu^-) &= (2.8^{+0.7}_{-0.6}) \times 10^{-9}, \\ \bar{\mathcal{B}}(B^0 \to \mu^+\mu^-) &= (3.9^{+1.6}_{-1.4}) \times 10^{-10}. \end{aligned} \qquad 19.$$

These measurements constitute the first observation of the $B_s^0 \to \mu^+\mu^-$ decay at more than 6σ and the first evidence for the $B^0 \to \mu^+\mu^-$ decay at more than 3σ. The results (**Figure 3**) are compatible with the SM at the level of $\sim 2\sigma$ and place strong constraints on possible BSM scalar and pseudoscalar operators, as discussed in Section 4.

The observation of the $B_s^0 \to \mu^+\mu^-$ decay and the first evidence for the $B^0 \to \mu^+\mu^-$ decay represent the culmination of an experimental search that lasted 30 years. Progress in finding the other dilepton modes has been somewhat less dramatic—as summarized in **Table 2**, the branching fraction limits are at least five orders of magnitude above the SM expectations. Prospects for improved measurements are discussed in Section 5.

3.2. Radiative Decays

As mentioned in Section 1, measurements of the $B \to X_s\gamma$ branching fraction, performed by BaBar (5, 6) and Belle (7), are consistent with the SM expectation (8). Therefore, the main focus in

Table 2 Theoretical predictions (84) and experimental results for time-integrated branching fractions of B meson decays to dilepton final states, $\bar{\mathcal{B}}[B^0_{(s)} \to \ell^+\ell^-]$[a]

Decay	Prediction	Measurement
$B^0 \to e^+e^-$	$(2.48 \pm 0.21) \times 10^{-15}$	$< 8.3 \times 10^{-8}$ (105)
$B^0_s \to e^+e^-$	$(8.54 \pm 0.55) \times 10^{-14}$	$< 2.8 \times 10^{-7}$ (105)
$B^0 \to \mu^+\mu^-$	$(1.06 \pm 0.09) \times 10^{-10}$	$(3.9^{+1.6}_{-1.4}) \times 10^{-10}$ (104)
$B^0_s \to \mu^+\mu^-$	$(3.65 \pm 0.23) \times 10^{-9}$	$(2.8^{+0.7}_{-0.6}) \times 10^{-9}$ (104)
$B^0 \to \tau^+\tau^-$	$(2.22 \pm 0.19) \times 10^{-8}$	$< 4.1 \times 10^{-3}$ (106)
$B^0_s \to \tau^+\tau^-$	$(7.73 \pm 0.49) \times 10^{-7}$	No result[b]

[a]Upper limits are at the 90% confidence level.
[b]The limit $\mathcal{B}(B^0_s \to \tau^+\tau^-) < 5.0\%$ has been derived (107) from ALEPH data (108).

this area has switched to ratios of processes mediated by $b \to d\gamma$ and $b \to s\gamma$ transitions, *CP* and isospin asymmetry measurements, and measurements of the polarization of the emitted photon.

The ratio of branching fractions for $b \to d\gamma$ and $b \to s\gamma$ mediated decays determines the ratio of CKM matrix elements $\left|V_{td}/V_{ts}\right|^2$ and is therefore of interest in searches for non-MFV BSM signatures. The measurement of the inclusive $\mathcal{B}(B \to X_d\gamma)$ is very challenging for any experiment but has nonetheless been performed by BaBar (109). Perhaps more promising is the possibility to use exclusive decays such as $\mathcal{B}(B^0 \to \rho^0\gamma)/\mathcal{B}(B^0 \to K^{*0}\gamma)$ (68, 69). Results presented by both BaBar (110) and Belle (111) provide a precision on $\left|V_{td}/V_{ts}\right|$ of ∼10%. Further reduction in the experimental uncertainty can be anticipated with results from LHCb (112), which has demonstrated its potential to reconstruct $B^0 \to K^{*0}\gamma$ by making the most precise determination of its *CP* asymmetry. Indeed, *CP* asymmetries of both inclusive and exclusive radiative b hadron decays offer powerful null tests of the SM (113), as do isospin asymmetries (i.e., differences between charged and neutral B meson decay rates) (114). All such measurements to date are consistent with the SM (**Table 3**).

The branching fractions of inclusive and exclusive $b \to s\gamma$ decays are proportional at leading order to the photon dipole operator squared, $|C_7|^2 + |C'_7|^2$, and are not sensitive to the handedness of the emitted photon. In the SM, photons produced in radiative b hadron decays are almost entirely left-handed due to the chiral nature of the charged-current interaction. The right-handed component is suppressed by the ratio $C'_7/C_7 \sim m_s/m_b$; the exact level of suppression is mode dependent due to QCD effects (69, 116). In many models that extend the SM, the virtual particles responsible for mediating the decay have no preferred left- or right-handed coupling, and the photon can be produced with a significantly lower degree of polarization. Well-known examples include supersymmetric models beyond MFV, left–right symmetric models, leptoquarks, and models with additional gauge bosons.

Table 3 Measurements of *CP* and isospin asymmetries in $b \to s\gamma$ transitions (19)[a]

Asymmetry	$B \to X_s\gamma$	$B \to K^*\gamma$
$\mathcal{A}_{CP}$	-0.015 ± 0.020	-0.002 ± 0.015
$\mathcal{A}_{\mathrm{I}}$	-0.01 ± 0.06	-0.012 ± 0.051

[a]The value of $\mathcal{A}_{CP}(B \to K^*\gamma)$ is the average for the B^0 decay, which is much more precise than the value for the B^+ decay. The value of $\mathcal{A}_{CP}(B \to X_s\gamma)$ is dominated by a result from BaBar (115).

Several methods to measure the photon polarization have been proposed. One of the most promising exploits the interference between B^0 and $\bar{B}^0$ decays when the hadronic system in the $B \to f\gamma$ decay is accessible to both. In such a case, the decay time–dependent asymmetry can be written as follows:

$$\mathcal{A}_{CP}(B \to f\gamma)(t) = S_{f\gamma} \sin(\Delta m t) - C_{f\gamma} \cos(\Delta m t), \quad 20.$$

where Δm is the mass difference in the B^0–$\bar{B}^0$ system. The *CP* asymmetry in the decay, $C_{f\gamma}$, has the same sensitivity as that measured with decay time–integrated methods, but the coefficient of the sinusoidal oscillation can be written as (117, 118)

$$S_{f\gamma} = \chi_f \sin(2\psi) \sin(2\beta), \quad 21.$$

where χ_f is the *C* eigenvalue of the hadronic system; $\tan\psi$ provides the magnitude of the ratio of right- and left-handed amplitudes; and $\beta \equiv \arg[-\frac{V_{cd}V_{cb}^*}{V_{td}V_{tb}^*}]$ is the angle of the CKM unitarity triangle, which has been measured to be $\sin(2\beta) = 0.682 \pm 0.019$ (19), assuming no NP in B^0–$\bar{B}^0$ oscillations. Measurements of $S_{f\gamma}$ can therefore be interpreted in terms of $\sin(2\psi)$ and, thus, in terms of C_7'/C_7.

BaBar and Belle have measured the coefficient $S_{K^*\gamma}$ using $B^0 \to K^{*0}\gamma$ decays, where $K^{*0} \to K_S^0\pi^0$. The result is (19, 119, 120)

$$S_{K^*\gamma} = -0.16 \pm 0.22, \quad 22.$$

which is consistent with the SM prediction of -0.02 (69). Measurements of similar coefficients in different final states are somewhat less precise, although the results for $B^0 \to K_S^0\rho^0\gamma$ are competitive (121, 122). Significant improvement in the sensitivity to right-handed currents is a key goal of current and future experiments.

The $B^0 \to K_S^0\pi^0\gamma$ decay is highly challenging to reconstruct at the LHC, but the production of all *b* hadron species opens alternative possibilities. Suggestions to measure the photon polarization using $\Lambda_b^0 \to \Lambda^{(*)}\gamma$ decays (123, 124) at the LHC have proved experimentally difficult due to the small polarization of Λ_b^0 baryons produced at the LHC (125). However, the $B_s^0 \to \phi\gamma$ decay appears attractive. Although the small SM value of $\beta_s \equiv -\arg[-\frac{V_{cs}V_{cb}^*}{V_{ts}V_{tb}^*}]$ suppresses the $S_{f\gamma}$ coefficient, the nonzero value of the width difference $\Delta\Gamma_s$ in the B_s^0–$\bar{B}_s^0$ system results in sensitivity to the photon polarization through the effective lifetime, or equivalently the $A^{\Delta\Gamma}$ parameter, of $B_s^0 \to \phi\gamma$ decays (126). An experimental advantage of such an analysis is that it does not require flavor tagging. LHCb (112) previously showed that it can reconstruct large yields of $B_s^0 \to \phi\gamma$ decays, and its first results on the effective lifetime are keenly anticipated.

Another way to probe C_7'/C_7 is through the photon direction with respect to the plane defined by the $\pi^+\pi^-$ system in $B^+ \to K^+\pi^-\pi^+\gamma$ decays (127–129). The so-called up–down asymmetry of the photon with respect to this plane is proportional to the photon polarization. The constant of proportionality suffers large hadronic uncertainties, which can, however, be controlled to some extent from data on $B^+ \to J/\psi K^+\pi^+\pi^-$ decays and other information concerning the $K\pi\pi$ system. LHCb (130) has performed a first measurement of this up–down asymmetry using its full Run I data set. The data are split into four regions of $K^+\pi^-\pi^+$ mass [$M(K^+\pi^-\pi^+)$] defined by the known $K^+\pi^-\pi^+$ resonances (**Figure 4**). Although nonzero photon polarization is observed at the 5.2σ level, when combining the four regions of $M(K^+\pi^-\pi^+)$, one needs a deeper understanding of the structure of the $K^+\pi^-\pi^+$ system to determine C_7'/C_7 with this approach.

The $B^0 \to K^{*0}\ell^+\ell^-$ decays can also be used to determine C_7'/C_7 at low dilepton invariant masses, where virtual photon contributions are expected to dominate. Study of the angular distributions enables determination of the parameter $A_\Gamma^{(2)}$ defined in Equation 12. At the limit

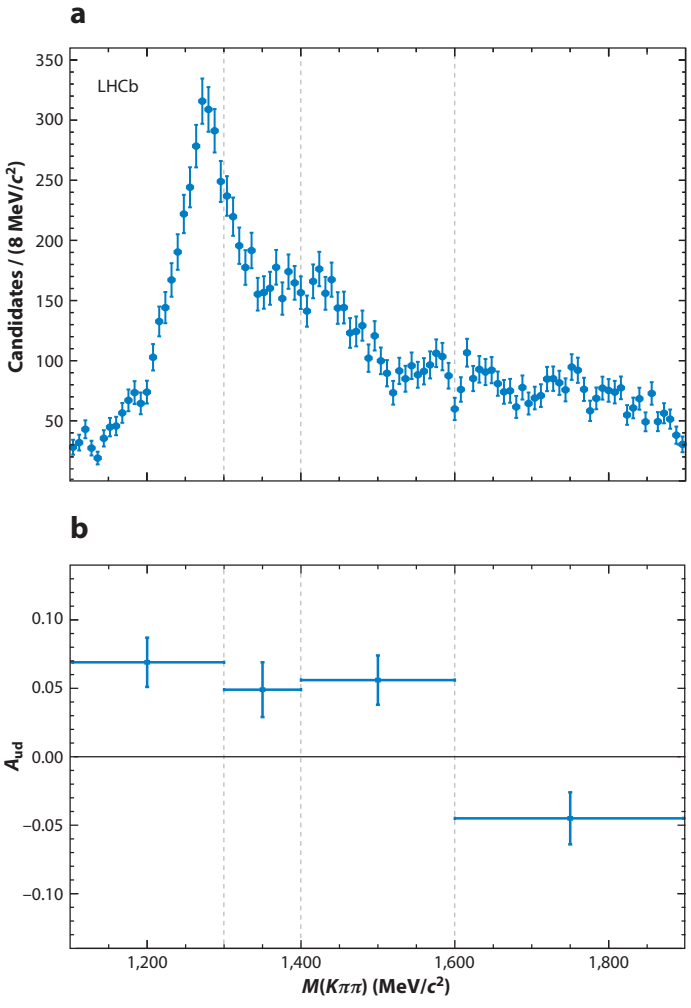

Erratum

Figure 4

(*a*) Background-subtracted $K^+\pi^-\pi^+$ invariant mass distribution in $B^+ \to K^+\pi^-\pi^+\gamma$ decays. (*b*) Up–down asymmetry (A_{ud}) in bins of $M(K^+\pi^-\pi^+)$. Modified from Reference 130.

$q^2 \to 0$, this quantity is directly sensitive to C_7'/C_7 (considering complex-valued Wilson coefficients, another observable A_T^{Im} probes the relative phase between C_7' and C_7). LHCb has studied $B^0 \to K^{*0}e^+e^-$ decays in the low-q^2 region (131, 132), obtaining

$$A_T^{(2)} = -0.23 \pm 0.23 \pm 0.05 \qquad 23.$$

for $0.002 < q^2 < 1.120\ \text{GeV}^2/c^4$ from the Run I data set.

3.3. Semileptonic $b \to s\ell^+\ell^-$ Decays

The LHC data have led to a wealth of results in semileptonic $b \to s\,\ell^+\ell^-$ decays. In the following subsections, we first consider results on branching fractions and rate asymmetries, and then discuss analyses of angular distributions.

Table 4 Branching fraction of the $B^+ \to K^+\mu^+\mu^-$ decay in selected q^2 bins $[q^2_{\min}, q^2_{\max}]$ (in GeV$^2/c^4$), from LHCb (143) compared with Standard Model (SM) predictions using light-cone-sum-rule (LCSR) (38) and lattice (40) calculations of form factors[a]

q^2 (GeV$^2/c^4$)	LHCb	SM (LCSR)	SM (lattice)
[1,6]	$(1.21 \pm 0.09 \pm 0.07) \times 10^{-7}$	$(1.75^{+0.60}_{-0.29}) \times 10^{-7}$	$(1.81 \pm 0.61) \times 10^{-7}$
[16,18]	$(0.35 \pm 0.04 \pm 0.02) \times 10^{-7}$	$(0.33^{+0.19}_{-0.09}) \times 10^{-7}$	$(0.39 \pm 0.04) \times 10^{-7}$

[a]The first uncertainty on the experimental results is statistical, and the second is systematic.

3.3.1. Branching fractions of semileptonic $b \to s\ell^+\ell^-$ decays. In contrast to the case of $b \to s\gamma$ decays, most of the experimental work on the $b \to s\ell^+\ell^-$ process has been with exclusive final states. Results on the inclusive decay (133, 134) have not yet reached high precision, but they will be important in the future. The LHC data have, however, led to a large increase in the yields of certain $b \to s\ell^+\ell^-$ decays, in particular those with a dimuon pair in the final state. As a result, there have been increasingly precise determinations of the branching fractions of the $B \to K\mu^+\mu^-$, $B \to K^*\mu^+\mu^-$, and $B^0_s \to \phi\mu^+\mu^-$ decays (135–138), as well as of the semileptonic b baryon decay $\Lambda^0_b \to \Lambda\mu^+\mu^-$ (139, 140). The theory input for the baryon decays (141, 142), in particular knowledge of the form factors, is not as well advanced as for the mesons, so they are not discussed further in this review.

The experimental results on the heavy-to-light branching fractions are now much more precise than the corresponding theoretical predictions, with further improved measurements anticipated in the coming years. This situation is illustrated in **Table 4**, which compares measurements of $\mathcal{B}(B^+ \to K^+\mu^+\mu^-)$ with theory predictions in the low- and high-q^2 regions. SM predictions for the branching fractions are sensitive to hadronic uncertainties in the form factors, which typically lead to uncertainties of $\mathcal{O}(30\%)$ on the SM predictions. Progress from lattice QCD has improved the precision in the high-q^2 region above the $\psi(3770)$ resonance, but the sensitivity to BSM physics remains limited by the uncertainty on the SM predictions.

In order to increase sensitivity to BSM physics, it is useful to study observables in which the effects of form factor uncertainties are reduced. Two such quantities are the *CP* asymmetry between B and $\bar{B}$ decays, $\mathcal{A}_{CP}$, and the isospin asymmetry between B^+ and B^0 decays, $\mathcal{A}_{\rm I}$. In the SM, the *CP* asymmetries of $B \to K^*\mu^+\mu^-$ and $B \to K\mu^+\mu^-$ decays are tiny, $\mathcal{O}(10^{-3})$, due to the small numerical size of the product of CKM elements $V_{ub}V^*_{us}$ compared with that of $V_{tb}V^*_{ts}$. Extensions of the SM can provide new sources of *CP* violation, so $\mathcal{A}_{CP}$ constitutes a null test of the SM, in which any visible direct *CP* violation would be evidence for BSM physics. The latest results, all consistent with the SM expectation of close to zero, are summarized in **Table 5**.

Table 5 Measurements of *CP* and isospin asymmetries in $B \to K^{(*)}\mu^+\mu^-$ transitions at low and high values of q^2 (135, 145)[a]

	$B \to K\mu^+\mu^-$		$B \to K^*\mu^+\mu^-$	
q^2 range	1.1–6.0	15.0–22.0	1.1–6.0	15.0–19.0
$\mathcal{A}_{CP}$	0.004 ± 0.028	-0.005 ± 0.030	-0.094 ± 0.047	-0.074 ± 0.044
$\mathcal{A}_{\rm I}$	$-0.10^{+0.08}_{-0.09} \pm 0.02$	$-0.09 \pm 0.08 \pm 0.02$	$0.00^{+0.12}_{-0.10} \pm 0.02$	$0.06^{+0.10}_{-0.09} \pm 0.02$

[a]Units of GeV$^2/c^4$ for q^2 are implied. Only results from LHCb are included because earlier, less precise measurements used a different q^2 binning scheme.

The decays appearing in the isospin asymmetry differ only by the flavor of the spectator quark in the B meson (u quark for the B^+ meson and d quark for the B^0). In the framework of the effective Hamiltonian, $\mathcal{A}_I$ differs from zero due to isospin-breaking effects in the form factors; from annihilation and exchange amplitudes; and from spectator scattering, where a virtual photon is emitted. The isospin asymmetry is expected to be $\sim -1\%$ at high q^2 in the SM (55), and for $B \to K^*$ decays it is expected to increase to $\sim +10\%$ as q^2 tends to zero (114, 144). Using its full Run I data set, LHCb (135) found that $\mathcal{A}_I$ in $B \to K$ and $B \to K^*$ decays is consistent with zero across the full q^2 window (**Table 5**).

The ratio of rates for $b \to d\ell^+\ell^-$ and $b \to s\ell^+\ell^-$ processes is sensitive to $|V_{td}/V_{ts}|^2$. The LHCb observation of the $B^+ \to \pi^+\mu^+\mu^-$ decay yields (146)

$$\begin{aligned} &\mathcal{B}(B^+ \to \pi^+\mu^+\mu^-) = [2.3 \pm 0.6\ (\text{stat.}) \pm 0.1\ (\text{syst.})] \times 10^{-8}, \\ &|V_{td}/V_{ts}| = 0.266 \pm 0.035\ (\text{stat.}) \pm 0.003\ (\text{syst.}), \end{aligned} \qquad 24.$$

where the uncertainty on $|V_{td}/V_{ts}|$ due to knowledge of the form factors, estimated to be 5.1%, is not included in the result. Further improvements, and observations of more $b \to d\ell^+\ell^-$ decay modes, are anticipated in the coming years.

3.3.2. Angular analyses of $b \to s\ell^+\ell^-$ decays. An angular analysis of $B \to K\ell^+\ell^-$ decays provides a simple null test of the SM (147). The angular distribution can be described by a single angle, θ_ℓ,

$$\frac{1}{\Gamma}\frac{\mathrm{d}\Gamma(B \to K\ell^+\ell^-)}{\mathrm{d}\cos\theta_\ell} = \frac{3}{4}(1 - F_H)(1 - \cos^2\theta_\ell) + \frac{1}{2}F_H + A_{FB}\cos\theta_\ell, \qquad 25.$$

with a constant term, $F_H/2$, and a forward–backward asymmetry, A_{FB}, that are linear in $\cos\theta_\ell$. Both F_H and A_{FB} are small within the SM, for $\ell = e$ or μ, and therefore can be used to probe the presence of BSM physics. In particular, these terms are sensitive to contributions from new scalar, pseudoscalar, and tensor operators. LHCb (148) has made precise measurements of these parameters in the decay $B^+ \to K^+\mu^+\mu^-$. The measurements are consistent with $A_{FB} = 0$ and $F_H \approx 0$, as expected in the SM.

The angular distribution of the $B^0 \to K^{*0}\mu^+\mu^-$ decay, with $K^{*0} \to K^+\pi^-$, is more complicated and can be described by three angles: θ_ℓ, which is defined by the direction of the μ^+ (μ^-) with respect to the B^0 ($\bar{B}^0$) in the dimuon rest frame; θ_K, which is defined by the direction of the kaon with respect to the B^0 ($\bar{B}^0$) in the K ($\bar{K}^{*0}$) rest frame; and ϕ, the angle between the plane containing the μ^+ and μ^- and the plane containing the kaon and pion. The differential decay rates in terms of these angles and the dimuon invariant mass squared, for B^0 and $\bar{B}^0$ decays, are given by

$$\begin{aligned} \frac{\mathrm{d}^4\Gamma(B^0 \to K^{*0}\mu^+\mu^-)}{\mathrm{d}\cos\theta_\ell\,\mathrm{d}\cos\theta_K\,\mathrm{d}\phi\,\mathrm{d}q^2} &= \frac{9}{32\pi}\sum\nolimits_i \bar{J}_i(q^2) f_i(\cos\theta_\ell, \cos\theta_K, \phi), \\ \frac{\mathrm{d}^4\Gamma(\bar{B}^0 \to \bar{K}^{*0}\mu^+\mu^-)}{\mathrm{d}\cos\theta_\ell\,\mathrm{d}\cos\theta_K\,\mathrm{d}\phi\,\mathrm{d}q^2} &= \frac{9}{32\pi}\sum\nolimits_i J_i(q^2) f_i(\cos\theta_\ell, \cos\theta_K, \phi). \end{aligned} \qquad 26.$$

Here, the $f_i(\cos\theta_\ell, \cos\theta_K, \phi)$ originate from spherical harmonics, and the J_i and $\bar{J}_i$ are bilinear combinations of K^{*0} decay amplitudes ($A_\parallel^{L,R}$, $A_\perp^{L,R}$, and $A_0^{L,R}$) (149). The CP-averaged observables,

$$S_i = (J_i + \bar{J}_i)/\frac{\mathrm{d}\left(\Gamma + \overline{\Gamma}\right)}{\mathrm{d}q^2}, \qquad 27.$$

depend on the underlying short-distance contributions from $C_7 \pm C_7'$, $C_9 \pm C_9'$ and $C_{10} \pm C_{10}'$, for CP-odd (CP-even) components. They can be related to the observables discussed in Section 2.3, for

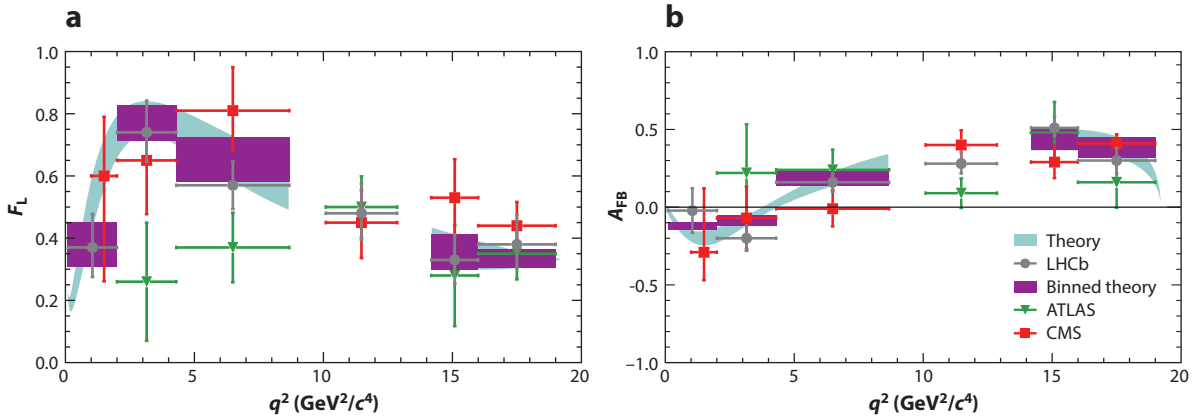

Figure 5

(*a*) Longitudinal polarization fraction (F_L) of K^{*0} mesons produced in $B^0 \to K^{*0}\mu^+\mu^-$ decays. (*b*) Dimuon system forward–backward asymmetry (A_{FB}). Results from ATLAS (153), CMS (137), and LHCb (136) are included. The data are overlaid with a Standard Model prediction (154).

example, by $S_3 = (1-F_L)A_T^{(2)}/2$, $S_{4,5} = \sqrt{F_L(1-F_L)}P'_{4,5}$. In addition, *CP*-violating observables ($\propto J_i - \bar{J}_i$), including several with high BSM sensitivity, can be obtained from the angular distributions (149–152).

Prior to data-taking at the LHC, the relatively modest samples of $B^0 \to K^{*0}\mu^+\mu^-$ candidates that were available meant that it was not possible to determine all of the terms of Equation 26. Instead, partial angular analyses of the decay were performed using single-angle projections. ATLAS (153), CMS (137), and LHCb (136) have also performed similar analyses that provide sensitivity to F_L, A_{FB} (**Figure 5**), and in the case of LHCb, $A_T^{(2)}$. Each of these observables is consistent with the SM expectation.

LHCb has also measured two of the "optimized" observables discussed in Section 2.3, P'_4 and P'_5 (155). In the low-q^2 region, there is a large local discrepancy between the data for P'_5 and the SM expectation at the 3.7σ level (**Figure 6**). This topic is discussed further in Section 4.

It is expected that full angular analyses of the $B^0 \to K^{*0}\mu^+\mu^-$ decay should be possible with the full Run I data sets of the LHC experiments. As the analyses become more precise and more complex, it will also be important to account for the contribution from the $K\pi$ S-wave under the K^{*0} peak (157–159). It will also be possible to determine *CP* asymmetries for each of the angular terms; these can then be used to constrain the imaginary parts of the Wilson coefficients. Other $B \to V\ell^+\ell^-$ decays, such as $B_s^0 \to \phi\mu^+\mu^-$, will provide additional constraints.

3.4. Nonuniversal Lepton Couplings

In the SM, with the notable exception of the Higgs boson, particles couple equally to the different flavors of lepton. The ratio of decay rates

$$R_H \equiv \frac{\Gamma(B \to H\,\mu^+\mu^-)}{\Gamma(B \to H\,e^+e^-)}, \qquad 28.$$

where $H = K, K^*, X_s$, and so on, is therefore expected to differ from unity only due to tiny Higgs penguin contributions and phase-space differences (160). Using the full Run I data set,

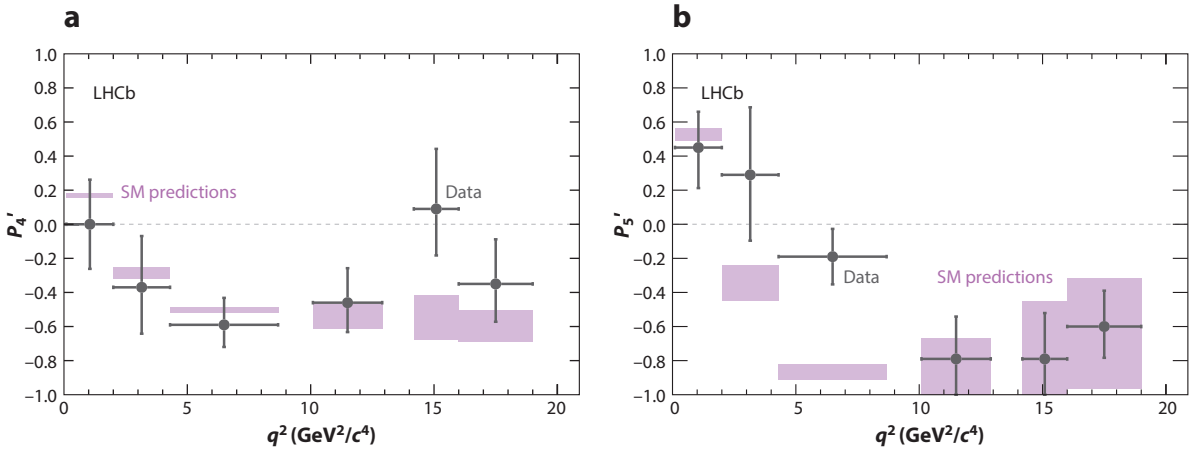

Figure 6

Observables (*a*) P_4' and (*b*) P_5', measured by LHCb (155) in $B^0 \to K^{*0}\mu^+\mu^-$ decays. The data are overlaid with a Standard Model (SM) prediction (156).

LHCb (161) measured the following value in the q^2 range $1 < q^2 < 6\,\mathrm{GeV}^2/c^4$:

$$R_K[1,6] = 0.745^{+0.090}_{-0.074}\,(\mathrm{stat.}) \pm 0.036\,(\mathrm{syst.}), \qquad 29.$$

which differs from the SM expectation of $R_K = 1.0003 \pm 0.0001$ (147) by 2.6σ. Although not yet at the level of significance that qualifies as evidence, this result has prompted theoretical speculation concerning possible sources of lepton nonuniversality, as discussed further in Section 4. Because results from BaBar on $B \to D^{(*)}\tau\nu$ decays (162, 163) also hint at violation of universality, this is a highly topical area.

3.5. Null Tests

Null tests of the SM, that is, searches for signals that are absent or vanishingly small in the SM, are valuable for several reasons. Observation of such a process would not only provide a smoking gun signature of BSM physics but would also indicate how the NP should be accommodated within the operator basis discussed in Section 2.1. In the absence of signals, limits can be placed on the contributions of the additional operators, which, when sufficiently stringent, justify the use of a restricted set of operators in model-independent analyses.

The tests of lepton universality discussed above fall into this category of null tests. It is also important to explore the possibility of LFV, and lepton number violation (LNV), in rare *b* hadron decays. The observation of neutrino oscillation demonstrates that lepton flavor is not an exact symmetry of nature, but if the SM is minimally expanded to allow neutrino mass, rates of processes with charged LFV remain unobservably small. Charged LFV (and LNV) does, however, arise in many BSM theories. Although strong limits exist from searches for rare muon and tau decays (for LFV) (164) and for neutrinoless double-β decay (for LNV) (165), there are models that respect those limits but nonetheless produce observable signatures in *b* hadron decays.

One of the most powerful of such LFV searches is for the $B^0_{(s)} \to e^\pm\mu^\mp$ decay. LHCb has improved the experimental limits to the level of $\lesssim 10^{-8}$ (166). The limit on the $B^0 \to e^\pm\mu^\mp$ decay is four orders of magnitude more stringent than those on $B^0 \to e^\pm\tau^\mp$ and $B^0 \to \mu^\pm\tau^\mp$ (167). For semileptonic decays, the limits on the $B^+ \to \pi^+e^\pm\mu^\mp$ and $B^+ \to K^+e^\pm\mu^\mp$ decays, at the level of

10^{-7} (168, 169), are similarly much more stringent than those on decays involving τ leptons (170). Because the operators can be written as being independent for each pair of leptons, it is important to improve all limits. These LFV semileptonic decay modes have not yet been investigated at the LHC.

Several searches have been performed for LNV in b hadron decays into final states containing a pair of same-sign leptons, $B^+ \to M^-\ell^+\ell'^+$. The strongest limits, from LHCb on $\mathcal{B}(B^+ \to \pi^-\mu^+\mu^+)$, are at the level of 10^{-9} (171). These are complemented by limits on numerous modes with different hadronic systems, $M^- = \pi^-, \rho^-, K^-, K^{*-}, D^-, D^{*-}, D_s^-, \ldots$, and in which one or both leptons may be an electron, all at the level of 10^{-6} or below (172–176). Limits also exist at the 10^{-6} level (177) on several b hadron decays that violate both baryon and lepton number, but these have not yet been explored at the LHC.

The most recent LHCb analysis of $B^+ \to \pi^-\mu^+\mu^+$ (171) set limits on the branching fraction as functions of the mass and decay time of the $\pi^-\mu^+$ pair. These results are of interest in probing models wherein the decay is mediated by the on-shell production of a Majorana neutrino, which could be long-lived. Similar experimental techniques can be used to search for long-lived particles (X) in $B \to KX$, with $X \to \ell^+\ell^-$, and similar decays. Such signatures are predicted in a range of theories that are generically referred to as dark sector models (178). Although these decays have not yet been investigated at the LHC, the possibility of searching for particles that travel $\mathcal{O}(1\text{ m})$ before decaying makes these probes complementary to other searches for new light resonances.

4. INTERPRETATION

4.1. Wilson Coefficient Fits

The observation of the $B_s^0 \to \mu^+\mu^-$ decay, described in Section 3.1, places strong constraints on scalar and pseudoscalar operators ($\mathcal{O}_S^{(\prime)}$ and $\mathcal{O}_P^{(\prime)}$). In BSM models, the $B_s^0 \to \ell^+\ell^-$ branching fraction is enhanced or suppressed by the ratio

$$\frac{\mathcal{B}(\bar{B}_s^0 \to \ell^+\ell^-)}{\mathcal{B}(\bar{B}_s^0 \to \ell^+\ell^-)_{\rm SM}} = |1 - 0.24(C_{10}^{\ell\,\rm NP} - C_{10}^{\ell'}) - y_\ell(C_P^\ell - C_P^{\ell'})|^2 + |y_\ell(C_S^\ell - C_S^{\ell'})|^2, \qquad 30.$$

where $y_\mu = 7.7$ and $y_e = (m_\mu/m_e)y_\mu = 1.6 \times 10^3$. At 1σ, the current experimental measurements imply (57)

$$|C_P^\mu - C_P^{\mu'}| \lesssim 0.3 \quad \text{and} \quad |C_S^\mu - C_S^{\mu'}| \lesssim 0.1. \qquad 31.$$

The constraints for dielectron decays are somewhat weaker,

$$|C_S^e - C_S^{e'}|^2 + |C_P^e - C_P^{e'}|^2 \lesssim 1.3, \qquad 32.$$

and substantial room still exists for ditau decays. Barring fortuitous cancellations that can happen if $C_S = C_S'$ and $C_P = C_P'$, visible effects from operators $\mathcal{O}_S^{(\prime)}$ and $\mathcal{O}_P^{(\prime)}$ to dimuon and dielectron decays can be neglected. Large accidental cancellations are also excluded by $B \to K\ell^+\ell^-$ decays, which constrain the combinations $|C_S + C_S'|$ and $|C_P + C_P'|$. Contributions from tensor operators are also constrained by $B \to K\ell^+\ell^-$ decays. In particular, the small size of the F_H term in the $B^+ \to K^+\mu^+\mu^-$ angular distribution (33) leads to a bound of

$$|C_T|^2 + |C_{T5}|^2 \lesssim 0.5. \qquad 33.$$

Therefore, it is appropriate to focus on the operator basis of Equation 2 and consider what the current measurements tell us about BSM contributions.

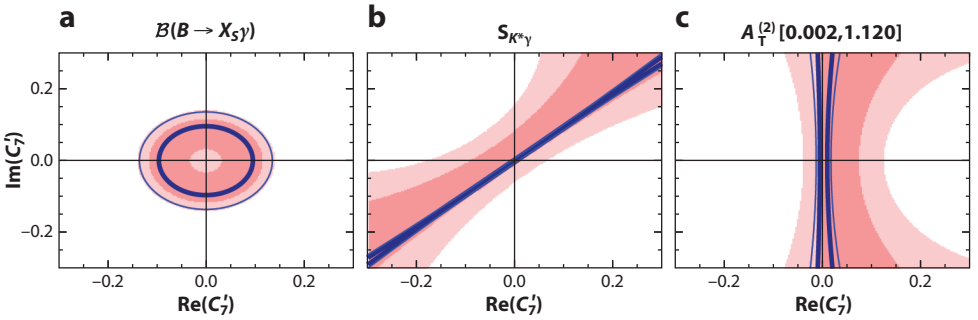

Figure 7

Dependence of the observables (*a*) $\mathcal{B}(B \to X_s\gamma)$, (*b*) $S_{K^*\gamma}$, and (*c*) $A_T^{(2)}$ on $\mathrm{Re}(C_7')$ and $\mathrm{Im}(C_7')$, computed using the EOS flavor tool (62), with all other Wilson coefficients fixed to their Standard Model expectations. The contours (*pink*) indicate the 68% and 90% intervals on experimental determinations of the observables. The lines indicate the theoretical uncertainty on each observable.

The rate of $B \to X_s\gamma$ decays is consistent with the SM and places constraints on the size of BSM contributions to the electromagnetic dipole operators $C_7^{(\prime)}$. The LHCb measurement of the up–down asymmetry in $B^+ \to K^+\pi^-\pi^+\gamma$ decays shows that the emitted photons are polarized, but further work is needed to interpret the asymmetry. Moreover, measurements of $S_{K^*\gamma}$ from BaBar and Belle are consistent with the SM expectation that $C_7 \gg C_7'$, but they are not yet sufficient to rule out a sizable right-handed polarization. **Figure 7** illustrates the current experimental constraints on C_7' after all of the other Wilson coefficients are fixed to their SM values. A future precise measurement of $A_T^{(2)}$ at low q^2 in the $B^0 \to K^{*0}e^+e^-$ decay, in combination with reduction on the uncertainty on $S_{K^*\gamma}$, would rule out a large right-handed contribution (179).

While C_7 and C_7' are consistent with their SM expectations, the situation with $C_{9,10}^{(\prime)}$ is more interesting. Measurements show that the rates of the $B \to K^{(*)}\mu^+\mu^-$ and $B_s^0 \to \phi\mu^+\mu^-$ decays tend to be below their SM expectations at both low and high q^2. The angular observable P_5' at low q^2 also appears to be discrepant with respect to the SM, although the other angular observables in the $B^0 \to K^{*0}\mu^+\mu^-$ decay are reasonably consistent with their SM expectations. **Figure 8** illustrates how these measurements relate to BSM contributions to C_9 and C_9'. In general, the data, although still consistent with the SM, are best described by a destructive BSM contribution to C_9, which both reduces the branching fraction of the semileptonic $b \to s\mu^+\mu^-$ decays and modifies the angular distribution of the $B^0 \to K^{*0}\mu^+\mu^-$ decay to be more consistent with the observed value of P_5' at low q^2. Global fits to $b \to s$ data favor $C_9^{\mathrm{NP}} \sim -1$; other NP parameters are consistent with zero or small additional contributions to C_9' or C_{10} (47, 180–183). Similar conclusions have been obtained from analyses that differ in statistical treatment, theoretical input (form factors), and the treatment of systematic uncertainties (incorporation of power corrections). A reduction in the rate of $b \to s\mu^+\mu^-$ processes could also be achieved by a contribution to C_{10} with the opposite sign to the SM ($C_{10}^{\mathrm{NP}} > 0$) (**Figure 9**). However, large BSM contributions to C_{10} are disfavored by the measured branching fraction of the $B_s^0 \to \mu^+\mu^-$ decay.

Current fits exhibit very little sensitivity to the phases of the Wilson coefficients $C_9^{(\prime)}$ and $C_{10}^{(\prime)}$ (154). This situation could be improved through the measurement of *CP* asymmetries in the $B^0 \to K^{*0}\mu^+\mu^-$ and $B_s^0 \to \phi\mu^+\mu^-$ angular distributions. Some of these asymmetries are naïve T-odd and hence do not require sizable strong phase differences between the decay amplitudes in order to be nonvanishing.

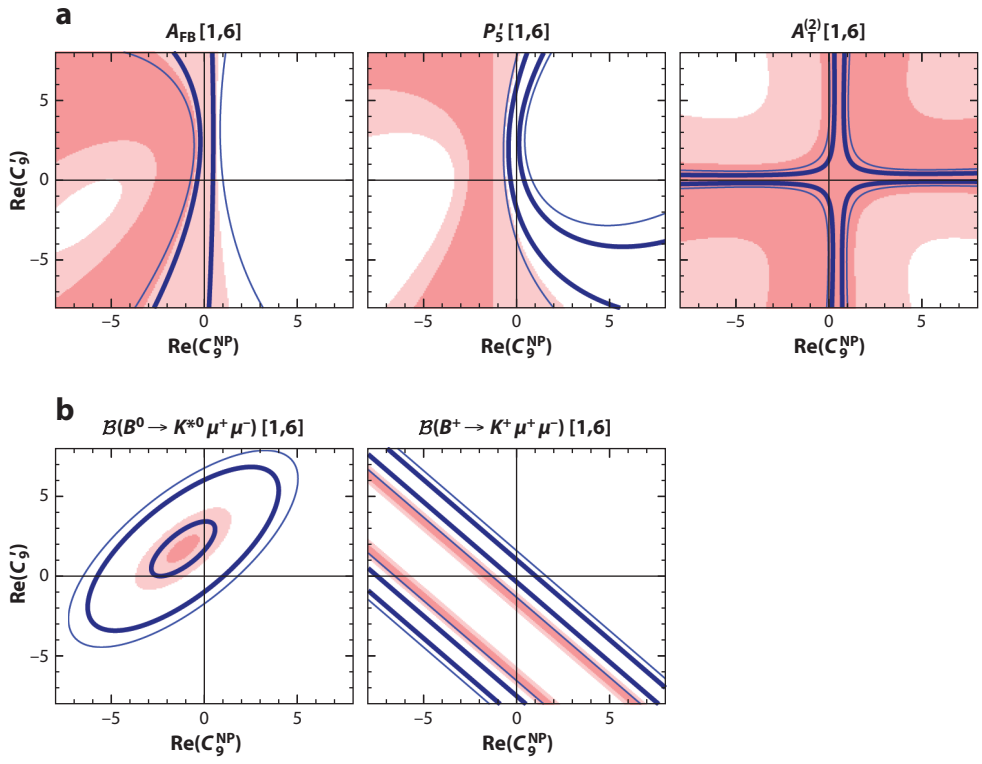

Figure 8

(*a*) Dependence of three angular observables, A_{FB}, P_5', and $A_T^{(2)}$, in the $B^0 \to K^{*0}\mu^+\mu^-$ decay in the q^2 range $1 < q^2 < 6\,\mathrm{GeV}^2/c^4$ on C_9^{NP} and C_9'. (*b*) Dependence of the branching fractions $\mathcal{B}(B^0 \to K^{*0}\mu^+\mu^-)$ and $\mathcal{B}(B^+ \to K^+\mu^+\mu^-)$ in the q^2 range $1 < q^2 < 6\,\mathrm{GeV}^2/c^4$; all values were computed using the EOS flavor tool (62), with all other Wilson coefficients fixed to their Standard Model expectations. The contours indicate the 68% and 90% intervals on experimental determinations of the observable. The lines indicate the theoretical uncertainty on each observable.

The measurement of R_K (Equation 29) raises the question of whether to consider only universal contributions to $C_{9,10}^{(\prime)}$. Considering flavor-dependent Wilson coefficients, the data imply

$$0.7 \lesssim \mathrm{Re}[X^e - X^\mu] \lesssim 1.5, \text{ where } X^\ell = C_9^{\mathrm{NP}\ell} + C_9^{\prime\ell} - (C_{10}^{\mathrm{NP}\,\ell} + C_{10}^{\prime\ell}), \quad \ell = e \text{ or } \mu. \qquad 34.$$

The anomaly could be caused by BSM physics that is suppressing the dimuon mode, enhancing the (currently less constrained) dielectron channel, or both. Interestingly, whereas the branching fraction of the $B^+ \to K^+\mu^+\mu^-$ decay is below the SM expectation, that of the $B^+ \to K^+e^+e^-$ decay is consistent with the prediction. The ratios R_K and R_{K^*} are interesting null tests of the SM because their theoretical predictions are free of hadronic uncertainties. In combination with the measurement of R_K, a measurement of R_{K^*}, or of the ratio of inclusive $b \to s\ell^+\ell^-$ branching fractions, R_{X_s}, could be used to separate nonuniversal BSM contributions to $C_{9,10}$ from those to $C_{9,10}'$ (184). For semileptonic decays with a ditau or dineutrino pair, the current data leave ample room for BSM contributions. In most models, however, correlations exist between the different lepton flavors, and indirect bounds on the couplings can be derived from the dimuon and dielectron data.

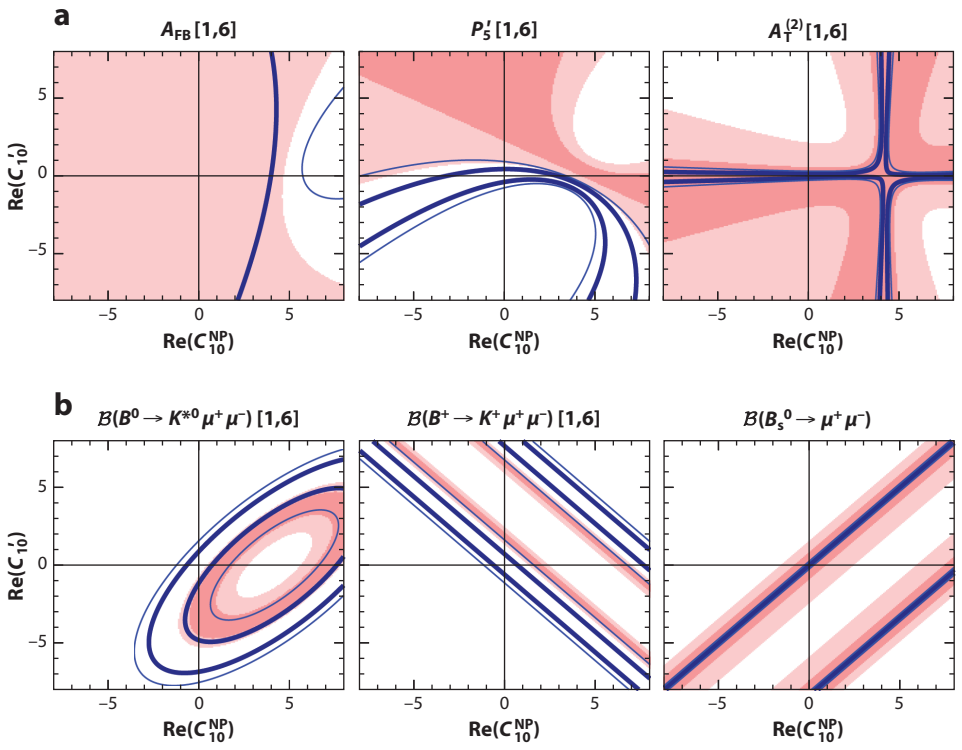

Figure 9

(*a*) Dependence of three angular observables, A_{FB}, P_5' and $A_T^{(2)}$, in the $B^0 \to K^{*0}\mu^+\mu^-$ decay in the q^2 range $1 < q^2 < 6\,\text{GeV}^2/c^4$ on C_{10}^{NP} and C_{10}'. (*b*) Dependence of the branching fractions $\mathcal{B}(B^0 \to K^{*0}\mu^+\mu^-)$ and $\mathcal{B}(B^+ \to K^+\mu^+\mu^-)$ in the q^2 range $1 < q^2 < 6\,\text{GeV}^2/c^4$ and of $\bar{\mathcal{B}}(B_s^0 \to \mu^+\mu^-)$; all values were computed using the EOS flavor tool (62), with all other Wilson coefficients fixed to their Standard Model expectations. The contours indicate the 68% and 90% intervals on experimental determinations of the observables. The lines indicate the theoretical uncertainty on each observable.

Global analyses of the $b \to s$ data have also been explored using the $SU(2)_L$ invariant basis described in Section 2.1 (183, 185, 186). These global fits have preference for a BSM contribution to $C_{LL} = C_9 - C_{10}$, with left-handed muons, as opposed to $C_{LR} = C_9 + C_{10}$.

Similar analyses of results on $b \to d$ decays are also possible, although the precision of the current data is not sufficient to obtain useful constraints. A comparison between $b \to d$ and $b \to s$ data allows one to search for non-MFV BSM signatures. Because violations of lepton universality may themselves be non-MFV signatures, if the hints of nonuniversality discussed above persist, it will become even more important to improve the precision of the constraints in the $b \to d$ sector.

4.2. Limits on New Physics Scales

In the SM, FCNC amplitudes for $|\Delta B| = |\Delta S| = 1$ transitions are suppressed because they occur through loop effects involving the weak scale [$g^2/(4\pi)^2$ and $1/M_W^2$] and also due to the smallness of the relevant CKM matrix elements, as shown by Equation 1. As discussed in Section 2.4, NP models may share some or all of these features. The assumed amount of suppression of BSM amplitudes influences the limits on the corresponding scales.

The best-fit values for $C_{9,10}^{\rm NP}$ can be interpreted in terms of a BSM scale $\Lambda_{\rm NP}$:

$$\Lambda_{\rm NP} \times \sqrt{|C_{9,10}^{\rm NP}|} \sim \begin{cases} \frac{4\pi\sqrt{2}M_{\rm W}}{g_e\sqrt{|V_{tb}V_{ts}^*|}} = 36\,{\rm TeV} & \text{(generic tree level)}, \\ \frac{\sqrt{2}M_{\rm W}}{e\sqrt{|V_{tb}V_{ts}^*|}} = 2\,{\rm TeV} & \text{(weak loop)}, \\ \sqrt{2}M_{\rm W}/e = 400\,{\rm GeV} & \text{(MFV, weak loop)}. \end{cases} \quad 35.$$

Thus, the value of $|C_9^{\rm NP}| = 1$ obtained in Section 4.1 corresponds to a value of $\Lambda_{\rm NP}$ ranging from ~400 GeV to ~36 TeV, depending on the model-dependent suppression of the BSM amplitude. For $|\Delta B| = |\Delta D| = 1$ transitions, the CKM suppression in the SM is stronger, and an analogous bound would imply a stronger constraint on $\Lambda_{\rm NP}$ in models without flavor suppression by $\sqrt{|V_{ts}/V_{td}|} \sim 2$.

If explicit flavor factors $\lambda\lambda^*$ are introduced for the BSM contribution, rare decays provide constraints on the combination $\lambda\lambda^*/\Lambda_{\rm NP}^2$. In contrast, B–$\bar{B}$ mixing constrains the combination $(\lambda\lambda^*)^2/\Lambda_{\rm NP}^2$. Similarly in the SM, the loop contribution to mixing is proportional to $G_{\rm F}|V_{tb}V_{ts}^*|^2$. Due to the stronger CKM suppression and in view of the strong constraints on *CP* violation in mixing, the resulting bounds on $\Lambda_{\rm NP}$ are typically more powerful than those from rare decays with two important exceptions. The first is where the $\Delta B = 1$ BSM amplitude arises at tree level, but the $\Delta B = 2$ BSM amplitude is loop induced, as in leptoquark models. Second, if the flavor suppression in the BSM model is sufficiently strong—that is, if $\lambda\lambda^*$ is small—then rare decays provide more stringent constraints on $\Lambda_{\rm NP}$. We emphasize that, due to the different dependence on scales and couplings, combinations of measurements of the $\Delta B = 1$ and $\Delta B = 2$ processes can be used to fix both dimensionful and dimensionless BSM parameters.

4.3. Impact on Model Building

The available data on rare b hadron decays place strong constraints on BSM contributions to the amplitudes, significantly affecting the range of models that can be considered. As discussed above, BSM effects in the Wilson coefficients of the semileptonic vector (C_9) and axial–vector operators (C_{10}) are now limited to be no larger than roughly one-third of their respective SM values, with constraints on the chirality-flipped coefficients ($C'_{9,10}$) of similar size. The Wilson coefficients of non-SM operators (scalars, tensors) are also strongly constrained, as shown in Equations 31 and 33. Note that these limits are for muons, and there is room left for possible signals in decays into other lepton species.

A common source of (pseudo)scalar operators in BSM models is Higgs-induced penguins. These processes are Yukawa dependent and, hence, couple differently to the different flavors of lepton. In the minimal supersymmetric Standard Model (MSSM) with MFV, the introduction of a second Higgs doublet can lead to an enhancement of $C_{\rm S}^\ell$ and $C_{\rm P}^\ell$ (93, 94):

$$C_{\rm S}^\ell \simeq -C_{\rm P}^\ell \propto m_\ell \tan^3\beta/m_A^2. \quad 36.$$

Here, $\tan\beta$ is the ratio of the vacuum expectation values for the two Higgs doublets present in the theory, and m_A is the mass of the *CP*-odd pseudoscalar Higgs boson. A sizable value of $\tan\beta$, ~15, can overcome the small muon mass factor. The constraints on $C_{\rm S}^\mu$ and $C_{\rm P}^\mu$ arising from the branching fraction of the $B_s^0 \to \mu^+\mu^-$ decay can therefore rule out significant amounts of the phase space of MSSM models (187).

Although the overall picture is one of consistency with the SM, there are some hints of anomalies in the $b \to s$ data that, if taken at face value, exhibit quite interesting features. Specifically,

there is (*a*) a preference for sizable NP in leptonic vector couplings, with axial–vector NP not larger in magnitude; (*b*) a preference for lepton nonuniversality; and (*c*) the possibility of right-handed currents. If future measurements substantiate any of these features, there will be huge implications for model building. Accommodating such features requires models that go beyond the most common and simple solutions to the hierarchy problem. For instance, features *b* and *c* directly imply a non-MFV flavor sector, and feature *b* also suggests LFV (80). Note that the significant level of nonuniversality suggested by the data, if confirmed, would rule out many proposed SM extensions, including the MSSM with *R*-parity conservation (188).

Feature *a* has inspired model-building with Z' extensions to the SM. As argued in Section 2.4, many models with possibilities for large Z penguins predict the hierarchy between NP in axial–vector and vector couplings to be the other way around. However, one popular approach that prefers large vector NP is the $SU(3) \times SU(3) \times U(1)$ (or 3-3-1) model (189, 190), which can also accommodate feature *c*. A model that can explain all three features is the gauged $L_\tau - L_\mu$ extension of the SM (76, 77). A variant of the latter with an additional Higgs doublet (191) can also explain the 2.5σ hint of Higgs boson decay to $\tau^\mp \mu^\pm$ (192). In this model, there are constraints on the ratio of the mass of the Z' boson and of its coupling, $m_{Z'}/g'$, in the few-TeV range.

Leptoquark models offer a natural framework to accommodate lepton nonuniversality. By choosing an $SU(2)_L$ triplet leptoquark that couples to muon doublets, one obtains a model that induces the following at tree level (33, 193):

$$C_9^{\mathrm{NP}\mu} = -C_{10}^{\mathrm{NP}\mu} = \frac{\pi}{\alpha_e} \frac{\lambda_{s\mu}^* \lambda_{b\mu}}{V_{tb} V_{ts}^*} \frac{\sqrt{2}}{2 M^2 G_F}, \qquad 37.$$

where M is the mass of the leptoquark. With benchmark values to explain the measurement of R_K given in Equation 29, $M^2 \simeq \lambda_{s\mu}^* \lambda_{b\mu}$ $(48\,\mathrm{TeV})^2$. Viable flavor structures for the leptoquark couplings $\lambda_{q\ell}$ can arise in models with partial compositeness (193). Dineutrino operators are induced, enhancing the branching ratios of $B \to K^{(*)} \nu \bar{\nu}$ and $B \to X_s \nu \bar{\nu}$ decays by a few percent. Corrections of a few percent to C_7 can also arise. The relation between axial–vector and vector coupling of Equation 37 can be broken if more than one leptoquark is introduced.

One may search for leptoquarks through their decays:

$$\phi^{2/3} \to t\nu, \quad \phi^{-1/3} \to b\nu, \quad t\mu^-, \quad \phi^{-4/3} \to b\mu^-, \qquad 38.$$

where the final-state particles must be from different generations because leptoquarks carry two generational indices. Such distinctive signatures, however, will be visible in experiments only if the leptoquarks are sufficiently light.

5. SUMMARY AND OUTLOOK

Run I of the LHC has led to a substantial improvement in precision in several key observables among rare decays of *b* hadrons. Particularly notable are the first observation of the very rare $B_s^0 \to \mu^+\mu^-$ decay and the wide range of kinematic observables now studied in $B^0 \to K^{*0}\mu^+\mu^-$ decays. The results remain broadly consistent with the SM, but deviations are present at an intriguing level of significance. In light of this situation, and considering the high sensitivity to BSM physics provided by rare *b* hadron decays, it is essential to continue to improve the precision.

Doing so presents challenges for both theory and experiment. An important task for theory is to reduce uncertainties that arise due to hadronic effects in the decays, including improving precision in decay constants and form factors through, for example, refined lattice QCD calculations. In the

case of $b \to s\ell^+\ell^-$ decays, another important challenge is to better understand power corrections and resonance contributions. Addressing these issues will require improved computations as well as detailed studies of data on specific observables and fits. The data will enable us not only to determine certain hadronic parameters but also to provide consistency checks and allow theoretical methods to be refined.

On the experimental side, the situation varies between b hadron decay modes. As shown in **Table 2**, the precision of branching fraction measurements of $B^0_{(s)} \to \ell^+\ell^-$ decays is not yet at the level of the theory predictions; only for $B^0_s \to \mu^+\mu^-$ is it within a factor of three. Improvements in these measurements can be achieved with a combination of experimental facilities. Data taking at the LHC, in Run II and beyond, will significantly increase the yields of dimuon decays. The experiments will benefit both from the increased cross section for the production of b quarks, which is expected to scale approximately linearly with the center-of-mass energy, and from the high luminosity. The increased yields will allow not only improved branching fraction measurements and a determination of their ratio but also a study of the effective lifetime in $B^0_s \to \mu^+\mu^-$ decays (194). The LHC experiments may also be able to improve the existing limits for the dielectron and ditau modes, but substantial improvement is more likely to be possible at the Belle II experiment (195) and at a very high luminosity $e^+e^- \to Z$ factory (196, 197), which have a more suitable experimental environment for these modes.

Radiative b hadron decays offer the potential for significant future improvement in our knowledge of right-handed contributions to the $b \to s\gamma$ dipole amplitude. Achieving this goal will require all of the methods most sensitive to the photon polarization to be used because they provide complementary information (179). These methods include time-dependent asymmetries in $B^0 \to K^0_S\pi^0\gamma$ and $B^0_s \to \phi\gamma$ decays, up–down asymmetries in $B^+ \to K^+\pi^+\pi^-\gamma$ decays, and angular asymmetries in $B^0 \to K^{*0}e^+e^-$ decays. Improved searches for *CP* violation in both inclusive and exclusive processes, as well as tests of MFV from $\mathcal{B}(B^0 \to \rho^0\gamma)/\mathcal{B}(B^0 \to K^{*0}\gamma)$, will also be important. There are excellent prospects for progress in all of these areas both at LHCb, including its upgrade (198), and at Belle II.

Data from the LHC have led to dramatic progress in experimental investigations into semileptonic $b \to s\ell^+\ell^-$ decays. The precision of the measurements of the differential branching fractions as a function of q^2 is now good enough that the focus is primarily on asymmetries, including *CP* asymmetries, isospin asymmetries, and lepton universality–violating differences in rates. With the increasing yields available in decay modes such as $B^0 \to K^{*0}\mu^+\mu^-$, full angular analyses are expected to become mandatory. It will also be possible to fit the data for *CP*-violating angular observables. The reconstruction of semileptonic modes with dielectron and ditau pairs is more challenging. The immediate objectives are to search for violations of lepton universality in a wide range of modes, including $B^0 \to K^{*0}e^+e^-$ and $B^0_s \to \phi e^+e^-$, and to begin searching for the ditau modes. In addition, high-luminosity e^+e^- experiments are expected to reach an interesting sensitivity to the $B \to K^{(*)}\nu\bar{\nu}$ decays, which provide complementary information on BSM physics because they are sensitive to other Wilson coefficients.

The main goals of ongoing investigations into rare b hadron decays are first to uncover evidence of BSM physics and then to deduce its nature. As discussed in this review, the quantity and quality of the data being produced by the LHC offer exciting prospects. The hints of BSM physics in the data analyzed so far have led to new directions in model building with the desired phenomenological features. Full use of the data that will be available from the LHC and from future experiments will require increased effort to identify and interpret patterns in the short-distance coefficients. Doing so will provide fantastic opportunities to learn about the problems and puzzles in fundamental physics that remain in the SM. This challenge can best be confronted by both theory and experiment in collaboration.

NOTE ADDED IN PROOF

After the completion of this review, preliminary results from the full analysis of the LHCb Run I data on the angular distributions of the $B \to K^* \mu^+ \mu^-$ decay became available (199). Careful study will be required before the detailed implications of these results are understood; however, consistency with the earlier results based on a subset of the data (136, 155) is seen. Therefore, the interpretation of the new data is likely to proceed along similar lines as discussed in this review.

DISCLOSURE STATEMENT

The authors are not aware of any affiliations, memberships, funding, or financial holdings that might be perceived as affecting the objectivity of this review.

ACKNOWLEDGMENTS

T.B. and T.G. thank the other members of the LHCb Collaboration for the enjoyable and productive teamwork that has led to many of the results discussed in this review. The writing of this review was supported in part by the Royal Society (T.B.), by the European Research Council under FP7 and the Science and Technology Facilities Council (T.G.), and by the Bundesministerium für Bildung und Forschung and the Deutsche Forschungsgemeinschaft Research Unit FOR 1873 "Quark Flavour Physics and Effective Field Theories" (G.H.). The authors thank Christoph Bobeth and Michal Kreps for useful comments.

LITERATURE CITED

1. Glashow SL, Iliopoulos J, Maiani L. *Phys. Rev. D* 2:1285 (1970)
2. Cabibbo N. *Phys. Rev. Lett.* 10:531 (1963)
3. Kobayashi M, Maskawa T. *Prog. Theor. Phys.* 49:652 (1973)
4. Alam MS, et al. (CLEO Collab.) *Phys. Rev. Lett.* 74:2885 (1995)
5. Lees JP, et al. (BaBar Collab.) *Phys. Rev. Lett.* 109:191801 (2012)
6. Lees JP, et al. (BaBar Collab.) *Phys. Rev. D* 86:112008 (2012)
7. Limosani A, et al. (Belle Collab.) *Phys. Rev. Lett.* 103:241801 (2009)
8. Misiak M, et al. *Phys. Rev. Lett.* 98:022002 (2007)
9. Aubert B, et al. (BaBar Collab.) *Phys. Rev. D* 81:051101 (2010)
10. Lees JP, et al. (BaBar Collab.) *Phys. Rev. D* 88:031102 (2013)
11. Hara K, et al. (Belle Collab.) *Phys. Rev. D* 82:071101 (2010)
12. Adachi I, et al. (Belle Collab.) *Phys. Rev. Lett.* 110:131801 (2013)
13. Kronenbitter B, et al. (Belle Collab.) arXiv:1503.05613 [hep-ex] (2015)
14. Evans L, Bryant P. *J. Instrum.* 3:S08001 (2008)
15. Aaij R, et al. (LHCb Collab.) *Phys. Lett. B* 694:209 (2010)
16. Aad G, et al. (ATLAS Collab.) *J. Instrum.* 3:S08003 (2008)
17. Chatrchyan S, et al. (CMS Collab.) *J. Instrum.* 3:S08004 (2008)
18. Alves AA Jr., et al. (LHCb Collab.) *J. Instrum.* 3:S08005 (2008)
19. Amhis Y, et al. (Heavy Flavor Aver. Group) arXiv:1412.7515 [hep-ex] (2014)
20. Nir Y, Gershon T. 2014. See Ref. 21, p. 223 (2014)
21. Olive KA, et al. (Part. Data Group) *Chin. Phys. C* 38:090001 (2014)
22. Borissov G, Fleischer R, Schune M-H. *Annu. Rev. Nucl. Part. Sci.* 63:205 (2013)
23. Artuso M, Meadows B, Petrov AA. *Annu. Rev. Nucl. Part. Sci.* 58:249 (2008)
24. Bryman D, Marciano WJ, Tschirhart R, Yamanaka T. *Annu. Rev. Nucl. Part. Sci.* 61:331 (2011)
25. Cirigliano V, et al. *Rev. Mod. Phys.* 84:399 (2012)
26. Chierici R. *Riv. Nuovo Cim.* 37:47 (2014)

27. Déliot F, Hadley N, Parke S, Schwarz T. *Annu. Rev. Nucl. Part. Sci.* 64:363 (2014)
28. Hurth T, Nakao M. *Annu. Rev. Nucl. Part. Sci.* 60:645 (2010)
29. Buchalla G, Buras AJ, Lautenbacher ME. *Rev. Mod. Phys.* 68:1125 (1996)
30. Chetyrkin KG, Misiak M, Munz M. *Phys. Lett. B* 400:206 (1997)
31. Bobeth C, Misiak M, Urban J. *Nucl. Phys. B* 574:291 (2000)
32. Alonso R, Grinstein B, Camalich JM. *Phys. Rev. Lett.* 113:241802 (2014)
33. Hiller G, Schmaltz M. *Phys. Rev. D* 90:054014 (2014)
34. Fox PJ, et al. *Phys. Rev. D* 78:054008 (2008)
35. Beneke M, Feldmann T, Seidel D. *Nucl. Phys. B* 612:25 (2001)
36. Grinstein B, Pirjol D. *Phys. Rev. D* 70:114005 (2004)
37. Khodjamirian A, Mannel T, Pivovarov AA, Wang Y-M. *J. High Energy Phys.* 09:089 (2010)
38. Khodjamirian A, Mannel T, Wang YM. *J. High Energy Phys.* 02:010 (2013)
39. Ball P, Zwicky R. *Phys. Rev. D* 71:014029 (2005)
40. Bouchard C, et al. (HPQCD Collab.) *Phys. Rev. D* 88:054509 (2013); Bouchard C, et al. (HPQCD Collab.) Erratum. *Phys. Rev. D* 88:079901 (2013)
41. Horgan RR, Liu Z, Meinel S, Wingate M. *Phys. Rev. D* 89:094501 (2014)
42. Detmold W, Lin C-JD, Meinel S, Wingate M. *Phys. Rev. D* 87:074502 (2013)
43. Briceño RA, Hansen MT, Walker-Loud A. *Phys. Rev. D* 91:034501 (2015)
44. Jäger S, Camalich JM. *J. High Energy Phys.* 05:043 (2013)
45. Descotes-Genon S, Hofer L, Matias J, Virto J. *J. High Energy Phys.* 12:125 (2014)
46. Jäger S, Camalich JM. arXiv:1412.3183 [hep-ph] (2014)
47. Beaujean F, Bobeth C, van Dyk D. *Eur. Phys. J. C* 74:2897 (2014)
48. Buchalla G, Isidori G, Rey SJ. *Nucl. Phys. B* 511:594 (1998)
49. Kruger F, Sehgal LM. *Phys. Lett. B* 380:199 (1996)
50. Ali A, Ball P, Handoko LT, Hiller G. *Phys. Rev. D* 61:074024 (2000)
51. Aaij R, et al. (LHCb Collab.) *Phys. Rev. Lett.* 111:112003 (2013)
52. Bai JZ, et al. (BES Collab.) *Phys. Rev. Lett.* 88:101802 (2002)
53. Ablikim M, et al. (BES Collab.) *Phys. Lett. B* 660:315 (2008)
54. Lyon J, Zwicky R. arXiv:1406.0566 [hep-ph] (2014)
55. Beylich M, Buchalla G, Feldmann T. *Eur. Phys. J. C* 71:1635 (2011)
56. Hiller G, Zwicky R. *J. High Energy Phys.* 03:042 (2014)
57. Bobeth C, Hiller G, van Dyk D. *Phys. Rev. D* 87:034016 (2013)
58. Bobeth C, Hiller G, van Dyk D, Wacker C. *J. High Energy Phys.* 01:107 (2012)
59. Kumar G, Mahajan N. arXiv:1412.2955 [hep-ph] (2014)
60. Kruger F, Matias J. *Phys. Rev. D* 71:094009 (2005)
61. Descotes-Genon S, Matias J, Ramon M, Virto J. *J. High Energy Phys.* 01:048 (2013)
62. Bobeth C, Hiller G, van Dyk D. *J. High Energy Phys.* 07:098 (2010)
63. Matias J, Serra N. *Phys. Rev. D* 90:034002 (2014)
64. Feng JL. *Annu. Rev. Nucl. Part. Sci.* 63:351 (2013)
65. Isidori G, Nir Y, Perez G. *Annu. Rev. Nucl. Part. Sci.* 60:355 (2010)
66. D'Ambrosio G, Giudice GF, Isidori G, Strumia A. *Nucl. Phys. B* 645:155 (2002)
67. Bobeth C, Ewerth T, Kruger F, Urban J. *Phys. Rev. D* 66:074021 (2002)
68. Ali A, Lunghi E, Parkhomenko AY. *Phys. Lett. B* 595:323 (2004)
69. Ball P, Jones GW, Zwicky R. *Phys. Rev. D* 75:054004 (2007)
70. Ali A, Parkhomenko AY, Rusov AV. *Phys. Rev. D* 89:094021 (2014)
71. Halkiadakis E, Redlinger G, Shih D. *Annu. Rev. Nucl. Part. Sci.* 64:319 (2014)
72. Arkani-Hamed N, Dimopoulos S. *J. High Energy Phys.* 06:073 (2005)
73. Giudice GF, Romanino A. *Nucl. Phys. B* 699:65 (2004); Giudice GF, Romanino A. Erratum. *Nucl. Phys. B* 706:487 (2005)
74. Fan J, Reece M, Ruderman JT. *J. High Energy Phys.* 11:012 (2011)
75. Buchalla G, Hiller G, Isidori G. *Phys. Rev. D* 63:014015 (2000)
76. Fox PJ, Liu J, Tucker-Smith D, Weiner N. *Phys. Rev. D* 84:115006 (2011)
77. Altmannshofer W, Gori S, Pospelov M, Yavin I. *Phys. Rev. D* 89:095033 (2014)

78. Buras AJ, Buttazzo D, Girrbach-Noe J, Knegjens R. *J. High Energy Phys.* 11:121 (2014)
79. Davidson S, Bailey DC, Campbell BA. *Z. Phys. C* 61:613 (1994)
80. Glashow SL, Guadagnoli D, Lane K. *Phys. Rev. Lett.* 114:091801 (2015)
81. de Medeiros Varzielas I, Hiller G. arXiv:1503.01084 [hep-ph] (2015)
82. De Bruyn K, et al. *Phys. Rev. D* 86:014027 (2012)
83. Buras AJ, Girrbach J, Guadagnoli D, Isidori G. *Eur. Phys. J. C* 72:2172 (2012)
84. Bobeth C, et al. *Phys. Rev. Lett.* 112:101801 (2014)
85. Aoki S, et al. *Eur. Phys. J. C* 74:2890 (2014)
86. Bazavov A, et al. (Fermilab Lattice Collab., MILC Collab.) *Phys. Rev. D* 85:114506 (2012)
87. McNeile C, et al. *Phys. Rev. D* 85:031503 (2012)
88. Na H, et al. *Phys. Rev. D* 86:034506 (2012)
89. Hermann T, Misiak M, Steinhauser M. *J. High Energy Phys.* 12:097 (2013)
90. Bobeth C, Gorbahn M, Stamou E. *Phys. Rev. D* 89:034023 (2014)
91. Huang C-S, Liao W, Yan Q-S. *Phys. Rev. D* 59:011701 (1999)
92. Choudhury SR, Gaur N. *Phys. Lett. B* 451:86 (1999)
93. Babu KS, Kolda CF. *Phys. Rev. Lett.* 84:228 (2000)
94. Bobeth C, Ewerth T, Kruger F, Urban J. *Phys. Rev. D* 64:074014 (2001)
95. Abazov VM, et al. (D0 Collab.) *Phys. Lett. B* 693:539 (2010)
96. Aaltonen T, et al. (CDF Collab.) *Phys. Rev. Lett.* 107:191801 (2011)
97. Aaij R, et al. (LHCb Collab.) *Phys. Lett. B* 699:330 (2011)
98. Aaij R, et al. (LHCb Collab.) *Phys. Lett. B* 708:55 (2012)
99. Aaij R, et al. (LHCb Collab.) *Phys. Rev. Lett.* 108:231801 (2012)
100. Chatrchyan S, et al. (CMS Collab.) *J. High Energy Phys.* 04:033 (2012)
101. Aad G, et al. (ATLAS Collab.) *Phys. Lett. B* 713:387 (2012)
102. Chatrchyan S, et al. (CMS Collab.) *Phys. Rev. Lett.* 111:101804 (2013)
103. Aaij R, et al. (LHCb Collab.) *Phys. Rev. Lett.* 111:101805 (2013)
104. Khachatryan V, et al. (CMS Collab., LHCb Collab.) *Nature*. doi:10.1038/nature14474 (2015)
105. Aaltonen T, et al. (CDF Collab.) *Phys. Rev. Lett.* 102:201801 (2009)
106. Aubert B, et al. (BaBar Collab.) *Phys. Rev. Lett.* 96:241802 (2006)
107. Grossman Y, Ligeti Z, Nardi E. *Phys. Rev. D* 55:2768 (1997)
108. Buskulic D, et al. (ALEPH Collab.) *Phys. Lett. B* 343:444 (1995)
109. del Amo Sanchez P, et al. (BaBar Collab.) *Phys. Rev. D* 82:051101 (2010)
110. Aubert B, et al. (BaBar Collab.) *Phys. Rev. D* 78:112001 (2008)
111. Taniguchi N, et al. (Belle Collab.) *Phys. Rev. Lett.* 101:111801 (2008)
112. Aaij R, et al. (LHCb Collab.) *Nucl. Phys. B* 867:1 (2013)
113. Kagan AL, Neubert M. *Phys. Rev. D* 58:094012 (1998)
114. Kagan AL, Neubert M. *Phys. Lett. B* 539:227 (2002)
115. Lees JP, et al. (BaBar Collab.) *Phys. Rev. D* 90:092001 (2014)
116. Grinstein B, Grossman Y, Ligeti Z, Pirjol D. *Phys. Rev. D* 71:011504 (2005)
117. Atwood D, Gronau M, Soni A. *Phys. Rev. Lett.* 79:185 (1997)
118. Atwood D, Gershon T, Hazumi M, Soni A. *Phys. Rev. D* 71:076003 (2005)
119. Aubert B, et al. (BaBar Collab.) *Phys. Rev. D* 78:071102 (2008)
120. Ushiroda Y, et al. (Belle Collab.) *Phys. Rev. D* 74:111104 (2006)
121. Li J, et al. (Belle Collab.) *Phys. Rev. Lett.* 101:251601 (2008)
122. Akar S. (BaBar Collab.) *J. Phys. Conf. Ser.* 556:012047 (2014)
123. Legger F, Schietinger T. *Phys. Lett. B* 645:204 (2007); Legger F, Schietinger T. Erratum. *Phys. Lett. B* 647:527 (2007)
124. Hiller G, Knecht M, Legger F, Schietinger T. *Phys. Lett. B* 649:152 (2007)
125. Aaij R, et al. (LHCb Collab.) *Phys. Lett. B* 724:27 (2013)
126. Muheim F, Xie Y, Zwicky R. *Phys. Lett. B* 664:174 (2008)
127. Gronau M, Grossman Y, Pirjol D, Ryd A. *Phys. Rev. Lett.* 88:051802 (2002)
128. Gronau M, Pirjol D. *Phys. Rev. D* 66:054008 (2002)
129. Kou E, Le Yaouanc A, Tayduganov A. *Phys. Rev. D* 83:094007 (2011)

130. Aaij R, et al. (LHCb Collab.) *Phys. Rev. Lett.* 112:161801 (2014)
131. Aaij R, et al. (LHCb Collab.) *J. High Energy Phys.* 05:159 (2013)
132. Aaij R, et al. (LHCb Collab.) *J. High Energy Phys.* 04:064 (2015)
133. Lees JP, et al. (BaBar Collab.) *Phys. Rev. Lett.* 112:211802 (2014)
134. Sato Y, et al. (Belle Collab.) arXiv:1402.7134 [hep-ex] (2014)
135. Aaij R, et al. (LHCb Collab.) *J. High Energy Phys.* 06:133 (2014)
136. Aaij R, et al. (LHCb Collab.) *J. High Energy Phys.* 08:131 (2013)
137. Chatrchyan S, et al. (CMS Collab.) *Phys. Lett. B* 727:77 (2013)
138. Aaij R, et al. (LHCb Collab.) *J. High Energy Phys.* 07:084 (2013)
139. Aaltonen T, et al. (CDF Collab.) *Phys. Rev. Lett.* 107:201802 (2011)
140. Aaij R, et al. (LHCb Collab.) *Phys. Lett. B* 725:25 (2013)
141. Böer P, Feldmann T, van Dyk D. *J. High Energy Phys.* 01:155 (2015)
142. Wang Y, Li Y, Lu C-D. *Eur. Phys. J. C* 59:861 (2009)
143. Aaij R, et al. (LHCb Collab.) *J. High Energy Phys.* 02:105 (2013)
144. Feldmann T, Matias J. *J. High Energy Phys.* 01:074 (2003)
145. Aaij R, et al. (LHCb Collab.) *J. High Energy Phys.* 09:177 (2014)
146. Aaij R, et al. (LHCb Collab.) *J. High Energy Phys.* 12:125 (2012)
147. Bobeth C, Hiller G, Piranishvili G. *J. High Energy Phys.* 12:040 (2007)
148. Aaij R, et al. (LHCb Collab.) *J. High Energy Phys.* 05:082 (2014)
149. Kruger F, Sehgal LM, Sinha N, Sinha R. *Phys. Rev. D* 61:114028 (2000); Kruger F, Sehgal LM, Sinha N, Sinha R. Erratum. *Phys. Rev. D* 63:019901 (2001)
150. Bobeth C, Hiller G, Piranishvili G. *J. High Energy Phys.* 07:106 (2008)
151. Egede U, et al. *J. High Energy Phys.* 10:056 (2010)
152. Alok AK, et al. *J. High Energy Phys.* 11:122 (2011)
153. ATLAS Collab. *ATLAS-CONF-2013-038*. **https://cds.cern.ch/record/1537961** (2013)
154. Bobeth C, Hiller G, van Dyk D. *J. High Energy Phys.* 07:067 (2011)
155. Aaij R, et al. (LHCb Collab.) *Phys. Rev. Lett.* 111:191801 (2013)
156. Descotes-Genon S, Hurth T, Matias J, Virto J. *J. High Energy Phys.* 05:137 (2013)
157. Becirevic D, Tayduganov A. *Nucl. Phys. B* 868:368 (2013)
158. Matias J. *Phys. Rev. D* 86:094024 (2012)
159. Blake T, Egede U, Shires A. *J. High Energy Phys.* 03:027 (2013)
160. Hiller G, Kruger F. *Phys. Rev. D* 69:074020 (2004)
161. Aaij R, et al. (LHCb Collab.) *Phys. Rev. Lett.* 113:151601 (2014)
162. Lees JP, et al. (BaBar Collab.) *Phys. Rev. Lett.* 109:101802 (2012)
163. Lees JP, et al. (BaBar Collab.) *Phys. Rev. D* 88:072012 (2013)
164. Marciano WJ, Mori T, Roney JM. *Annu. Rev. Nucl. Part. Sci.* 58:315 (2008)
165. Avignone FT, Elliott SR, Engel J. *Rev. Mod. Phys.* 80:481 (2008)
166. Aaij R, et al. (LHCb Collab.) *Phys. Rev. Lett.* 111:141801 (2013)
167. Aubert B, et al. (BaBar Collab.) *Phys. Rev. D* 77:091104 (2008)
168. Aubert B, et al. (BaBar Collab.) *Phys. Rev. D* 73:092001 (2006)
169. Aubert B, et al. (BaBar Collab.) *Phys. Rev. Lett.* 99:051801 (2007)
170. Lees JP, et al. (BaBar Collab.) *Phys. Rev. D* 86:012004 (2012)
171. Aaij R, et al. (LHCb Collab.) *Phys. Rev. Lett.* 112:131802 (2014)
172. Aaij R, et al. (LHCb Collab.) *Phys. Rev. D* 85:112004 (2012)
173. Seon O, et al. (Belle Collab.) *Phys. Rev. D* 84:071106 (2011)
174. Liventsev D, et al. (Belle Collab.) *Phys. Rev. D* 87:071102 (2013)
175. Lees JP, et al. (BaBar Collab.) *Phys. Rev. D* 85:071103 (2012)
176. Lees JP, et al. (BaBar Collab.) *Phys. Rev. D* 89:011102 (2014)
177. del Amo Sanchez P, et al. (BaBar Collab.) *Phys. Rev. D* 83:091101 (2011)
178. Essig R, et al. arXiv:1311.0029 [hep-ph] (2013)
179. Becirevic D, Kou E, Le Yaouanc A, Tayduganov A. *J. High Energy Phys.* 08:090 (2012)
180. Descotes-Genon S, Matias J, Virto J. *Phys. Rev. D* 88:074002 (2013)
181. Hurth T, Mahmoudi F. *J. High Energy Phys.* 04:097 (2014)

182. Altmannshofer W, Straub DM. *Eur. Phys. J. C* 73:2646 (2013)
183. Altmannshofer W, Straub DM. arXiv:1411.3161 [hep-ph] (2014)
184. Hiller G, Schmaltz M. *J. High Energy Phys.* 02:055 (2015)
185. Ghosh D, Nardecchia M, Renner SA. *J. High Energy Phys.* 12:131 (2014)
186. Hurth T, Mahmoudi F, Neshatpour S. *J. High Energy Phys.* 12:053 (2014)
187. Kowalska K, Roszkowski L, Sessolo EM. *J. High Energy Phys.* 06:078 (2013)
188. Martin SP. *Adv. Ser. Direct. High Energy Phys.* 21:1 (2010)
189. Gauld R, Goertz F, Haisch U. *J. High Energy Phys.* 01:069 (2014)
190. Buras AJ, De Fazio F, Girrbach J. *J. High Energy Phys.* 02:112 (2014)
191. Crivellin A, D'Ambrosio G, Heeck J. *Phys. Rev. Lett.* 114:151801 (2015)
192. CMS Collab. *CMS-PAS-HIG-14-005*. **https://cds.cern.ch/record/1740976** (2014)
193. Gripaios B, Nardecchia M, Renner SA. arXiv:1412.1791 [hep-ph] (2014)
194. De Bruyn K, et al. *Phys. Rev. Lett.* 109:041801 (2012)
195. Aushev T, et al. arXiv:1002.5012 [hep-ex] (2010)
196. Zhao Z-G, et al. *eConf C* 010630:e2001 (2001)
197. Bicer M, et al. (TLEP Design Study Work. Group) *J. High Energy Phys.* 01:164 (2014)
198. Aaij R, et al. (LHCb Collab.) *Eur. Phys. J. C* 73:2373 (2013)
199. LHCb Collab. *LHCb-CONF-2015-002*. **https://cds.cern.ch/record/2002772** (2015)